Published in Geochemistry, Geophysics, Geosystems 18 (2017)
doi:10.1002/2016GC006477

Mineralogical, geochemical and magnetic signatures of surface sediments from the Canadian Beaufort Shelf and Amundsen Gulf (Canadian Arctic)

Adriana Gamboa [1,4,5], Jean-Carlos Montero-Serrano [1,3*], Guillaume St-Onge [2,3], André Rochon [1,3], Pierre-Arnaud Desiage [1,2,3]

[1] Institut des sciences de la mer de Rimouski, Université du Québec à Rimouski, 310 allée des Ursulines, Rimouski, Québec, G5L 3A1, Canada

[2] Canada Research Chair in Marine Geology, Institut des sciences de la mer de Rimouski, Université du Québec à Rimouski, 310 allée des Ursulines, Rimouski, Québec, G5L 3A1, Canada

[3] GEOTOP Research Center, C.P. 8888, Succursale Centre-ville, Montréal, QC H3C 3P8, Canada

[4] Postgrado en Ciencias Marinas, Instituto Oceanográfico de Venezuela, Universidad de Oriente, Cumaná, 6101 A, Venezuela

[5] Coordinación de Procesos Químicos. Universidad Politécnica del Oeste de Sucre «Clodosbaldo Russián» Cumaná, 6101 A, Venezuela

[*] Corresponding author: J.-C. Montero-Serrano. Phone: +1.418.723.1986 Ext: 1139; Fax: +1.418.724.1842; E-mail address: jeancarlos_monteroserrano@uqar.ca

Highlights

1. Tracking sediment provenance in the Canadian Beaufort Shelf and Amundsen Gulf
2. Coupling grain size, mineralogical, geochemical and magnetic proxies in the western Canadian Arctic
3. Dolomite–K-feldspar and Ca-Mg characterize southwestern Banks Island
4. Phyllosilicates–magnetite–Fe-oxides and Al-K-Ti-Fe-Cr-V-Zn-P characterize the Canadian Beaufort Shelf
5. The Canadian Beaufort Shelf and Amundsen Gulf are separated into four sedimentological provinces

Abstract

Mineralogical, geochemical, magnetic, and siliciclastic grain-size signatures of 34 surface sediment samples from the Mackenzie-Beaufort Sea Slope and Amundsen Gulf were studied in order to better constrain the redox status, detrital particle provenance, and sediment dynamics in the western Canadian Arctic. Redox-sensitive elements (Mn, Fe, V, Cr, Zn) indicate that modern sedimentary deposition within the Mackenzie-Beaufort Sea Slope and Amundsen Gulf took place under oxic bottom-water conditions, with more turbulent mixing conditions and thus a well-oxygenated water column prevailing within the Amundsen Gulf. The analytical data obtained, combined with multivariate statistical (notably, principal component and fuzzy c-means clustering analyses) and spatial analyses, allowed the division of the study area into four provinces with distinct sedimentary compositions: (1) the Mackenzie Trough-Canadian Beaufort Shelf with high phyllosilicate-Fe oxide-magnetite and Al-K-Ti-Fe-Cr-V-Zn-P contents; (2) Southwestern Banks Island, characterized by high dolomite–K-feldspar and Ca-Mg-LOI contents; (3) the Central Amundsen Gulf, a transitional zone typified by intermediate phyllosilicate–magnetite–K-feldspar–dolomite and Al-K-Ti-Fe-Mn-V-Zn-Sr-Ca-Mg-LOI contents; and (4) mud volcanoes on the Canadian Beaufort Shelf distinguished by poorly sorted coarse-silt with high quartz-plagioclase-authigenic carbonate and Si-Zr contents, as well as high magnetic susceptibility. Our results also confirm that the present-day sedimentary dynamics on the Canadian Beaufort Shelf is mainly controlled by sediment supply from the Mackenzie River. Overall, these insights provide a basis for future studies using mineralogical, geochemical, and magnetic signatures of Canadian Arctic sediments in order to reconstruct past variations in sediment inputs and transport pathways related to late Quaternary climate and oceanographic changes.

Keywords: mineralogy; elemental geochemistry; magnetic properties; surface sediment; sediment provenance; redox condition; Canadian Beaufort Shelf; Amundsen Gulf.

1. Introduction

Sedimentation in the Arctic Ocean is characterized by high terrigenous input from the surrounding continents with different petrographic signatures (Harrison et al., 2011). These sediments are delivered into the Arctic Ocean mainly as suspended particulate matter and bed loads from several large river systems (notably, the Mackenzie, Kolyma, Lena, Ob, Yenisei, Pechora, and Severnaya Dvina; Holmes et al., 2002; Wagner et al., 2011) and from coastal erosion, and then dispersed by ocean currents (summarized in Stein, 2008). Furthermore, in shallow margins, suspended terrigenous particles can also be incorporated in sea ice during its formation and then be transported via ocean currents over long distances throughout the Arctic Ocean, to finally settle far from their source of origin (e.g., Bischof et al., 1996; Darby et al., 2012, 2006).

Taking this into account, a number of studies have characterized the mineralogical and geochemical composition of the detrital sediments over the continental shelf from the Eurasian Basin (e.g., Vogt, 1997; Schoster et al., 2000; Viscosi-Shirley et al., 2003; Stein, 2008; Bazhenova, 2012), Chukchi Sea-Bering Strait (e.g., Asahara et al., 2012; Linsen et al., 2014), and Chukchi-Alaskan margin (e.g., Naidu et al., 1982; Naidu and Mowatt, 1983; Ortiz et al., 2009; Darby et al., 2012) to decipher: (1) variations in detrital particle provenance, (2) climate and atmospheric circulation changes in the source areas on adjacent landmasses, and (3) changes in sediment propagation and ocean-current pathways. However, few studies provide a general view of the surface detrital provenances and sediment-dispersal patterns within the Mackenzie-Beaufort Sea Slope and Amundsen Gulf (e.g., Naidu et al., 1971; Bornhold et al., 1975; Pelletier, 1975; Davidson et al., 1988; Hill et al., 1991; Darby et al., 2011; Vonk et al., 2015) compared to other Arctic continental shelf regions. To our knowledge, no general mineralogical and geochemical distributions of the Canadian Beaufort Shelf and Amundsen Gulf are available today. Such studies may provide a baseline to better interpret, in terms of sediment dynamics and climate change, the mineralogical and geochemical signatures preserved in the southern Beaufort

Sea sedimentary records, which may then help to place current western Arctic climate change (e.g., Kwok et al., 2009) into its broader context.

In this study, a multi-proxy analysis was carried out on the bulk detrital fraction of surface sediment samples from the Mackenzie-Beaufort Sea Slope and Amundsen Gulf in order to: (1) characterize the spatial distribution patterns of siliciclastic grain size, magnetic properties, bulk minerals, and elemental geochemistry in surface sediments; (2) identify different sedimentary provinces, source areas, and transport pathways of terrigenous material; and (3) better constrain modern sediment dynamics within the western Canadian Arctic. Overall, this study provides a unique opportunity to compare mineralogical, geochemical, magnetic, and siliciclastic grain-size signatures within the Mackenzie-Beaufort Sea Slope and Amundsen Gulf area.

2. Environmental setting

2.1. Regional morphology

The Canadian Beaufort Shelf is a shallow platform located along the northwestern Canadian coast in the southeastern Beaufort Sea (western Arctic Ocean; Figure 1). It is bordered to the west by the Mackenzie Trough and to the east by the Amundsen Gulf. This shelf is cut by several partially infilled cross-shelf channels: the Ikit Trough, the Kugmallit Channel, and the Niglik Channel (Blasco et al., 2013). Moreover, several hundreds of conical mounds, locally referred to as pingo-like-features (Shearer et al., 1971), occur across the Canadian Beaufort Shelf (Blasco et al., 2013). Based on seismic reflection profiles, water column acoustic anomalies (Paull et al., 2007; Blasco et al., 2013; Saint-Ange et al., 2014; Paull et al., 2015) together with geochemical composition of pore waters, gas and sediments (Paull et al., 2015), these conical features are now regarded as mud volcanoes. On the other hand, the Amundsen Gulf is a large channel (400-km-long, 200-km-wide, average water depth of 300 m; Stokes et

al., 2006) that connects the southeastern Beaufort Sea to the Canadian Arctic Archipelago (Figure 1). It is bordered by the Banks Island Shelf to the north and by the Mackenzie Shelf to the southwest.

The Canadian Beaufort Shelf and Amundsen Gulf are nearly completely covered by sea ice (pack-ice and landfast ice) from September/October to May (Barber and Hanesiak, 2004; Galley et al., 2008), with great annual and interannual variability (e.g., Schell et al., 2008; Bringué and Rochon, 2012). In summer, freshet from the Mackenzie River, wind forcing, and rising air temperatures result in ice-free conditions over the shelf by late July and over the slope in August (O'Brien et al., 2006). In addition, in the middle of landfast ice from Amundsen Gulf, the ice-free zone forms part of the Cape Bathurst Polynya which develops during winter at approximately the same location under the action of winds, currents and upwellings of warmer water (Arrigo and van Dijken, 2004). In this ice-free area, stronger westerly to northwesterly winds induce turbulent mixing of the water column (e.g., Magen, 2007; Forest et al., 2008; Tremblay et al., 2014).

2.2. Surrounding geology

The Mackenzie River drainage basin covers a large part of western Canada (~1.8×10^6 km^2; Carson et al., 1998; Hill et al., 2001). Three main geological units characterize the Mackenzie River basin (Millot et al., 2003): (1) the North American Cordillera (including the Rocky and the Mackenzie Mountains) in the western part, distinguished by volcanic and immature volcano-clastic sediments in the western Canadian orogenic belt (Stikine terrane) and carbonates and slates in the Mackenzie Mountains; (2) the Interior Platform (lowlands), composed of marine and non-marine sedimentary rocks (Cambrian to Cretaceous limestones, shales, and sandstones); and (3) the Canadian Shield in the eastern part, typified by old silicate rocks (Archean granites and gneisses) from the Slave Province (Padgham and Fyson, 1992). In turn, Banks Island is composed of Cretaceous shale and sandstone, Upper Devonian

sandstone and shale, and Tertiary–Quaternary glacial deposits, which are rich in dolomite clasts as well as quartz and feldspar grains (Bischof et al., 1996; Bischof and Darby, 1999).

2.3. Sedimentation

The Mackenzie River is the fourth-largest (after the Yenisei, Lena, and Ob rivers) Arctic river in terms of freshwater discharge (~420 km^3/yr; Wagner et al., 2011), but the first in terms of sediment discharge (~127 Mt/yr; Carson et al., 1998). This large suspended sediment discharge of the Mackenzie River forms a large sediment plume (generally 2–3 m thick; Hill et al., 1991) on the Canadian Beaufort Shelf (Figure 1). The transport of suspended sediments within this plume is affected by the ice cover, winds, and currents (Carmack and Macdonald, 2002). In winter, the Mackenzie River discharges are trapped on the inner shelf by the stamukhi (a field of ice fragments), which acts as an inverted dam and causes the formation of the "floating freshwater" lake Herlinveaux (Macdonald et al., 1995). In summer, the plume's position is greatly affected by prevailing winds, with winds from the northwest pushing the plume along Tuktoyaktuk Peninsula (Giovando and Herlinveaux, 1981), and winds from the southeast pushing the plume westward, beyond the Mackenzie Trough (MacNeil and Garrett, 1975). In addition, although coastal erosion is an important local sediment supply near the shoreline, its estimated contribution (~7 Mt/yr) is dwarfed by that of the Mackenzie River (Carmack and Macdonald, 2002). Furthermore, the suspended particulate matter supply to the Amundsen Gulf is much smaller than to the Canadian Beaufort shelf as no large rivers discharge into the Gulf (Macdonald et al., 1998). Indeed, small rivers located to the east Mackenzie River, such as the Anderson, Horton and Hornaday Rivers (Figure 1), have a weak mean annual freshwater discharge (<146 m^3/s; R-ArcticNet database: http://www.r-arcticnet.sr.unh.edu/v4.0/index.html; Lammers et al., 2001), and therefore, contribute weakly to the sedimentation in the eastern Mackenzie Shelf and Amundsen Gulf. Consequently, modern sedimentation rates are high within the Mackenzie Trough (~40–320 cm/ka; Macdonald et al., 1998;

Richerol et al., 2008a; Durantou et al., 2012) and on the nearby continental shelf and slope (~100–200 cm/ka; Barletta et al., 2008; Scott et al., 2009; Bringué and Rochon, 2012). To the east, these modern sedimentation rates decrease towards Amundsen Gulf (<80 cm/ka; Macdonald et al., 1998; Schell et al., 2008), where sediment hardly accumulates at all (Hill et al., 1991).

On the Canadian Beaufort shelf, most of the surficial seabed sediments are predominantly composed of Holocene marine olive-grey silts and clays (e.g., Pelletier, 1975; Hill et al., 1991; Barletta et al., 2008; Scott et al., 2009). Surface sediments from the Amundsen Gulf are composed of a relatively thin layer of olive-grey silty clay overlying a diamicton of brownish red color with abundant pebbles and cobbles (Bennett et al., 2008; Schell et al., 2008; Scott et al., 2009).

2.4. Oceanic circulation

Oceanic circulation in the southeastern Beaufort Sea is dominated by the anticyclonic Beaufort Gyre (BG), which pushes both surface currents and sea-ice westward at the shelf break (Figure 1). Conversely, closer to shore around the 50-m isobath, the Beaufort Undercurrent transports both Pacific and Atlantic waters eastwards along the continental margin and into Amundsen Gulf (e.g., Aagaard, 1984; Pickart, 2004; Bringué and Rochon, 2012; Durantou et al., 2012). In general, surface waters influenced by the anticyclonic BG enter Amundsen Gulf near southwestern Banks Island and exit near Cape Bathurst (Lanos, 2009). At a regional level, these surface circulation regimes are mainly controlled by changes in the phase of large-scale atmospheric patterns such as the Arctic Oscillation (AO; Darby et al., 2001; Macdonald et al., 2005) and the Pacific Decadal Oscillation (PDO; Overland et al., 1999; Durantou et al., 2012), which are both significant natural patterns in global climate variability.

3. Material and methods

3.1. Samples

A total of 34 surface sediment samples were collected at different depths in the Canadian Beaufort Shelf and Amundsen Gulf on board the Canadian Coast Guard Ship (CCGS) Amundsen during the CASES (Canadian Arctic Shelf Exchange Study) 2004 expedition (Rochon and onboard participants, 2004). The sampling was performed using a box core sampler (0.5 m x 0.5 m x 0.5 m) wherein the uppermost 5 mm of sediment was recovered in order to collect only the sediment-water interface (Richerol et al., 2008b). Based on the regional morphology, mud volcanoes distribution (Blasco et al., 2013), and the influence of the Mackenzie River plume (Richerol et al., 2008b; Scott et al., 2008), the surface sediment samples were divided into four main geographical areas (Figure 1): (1) Mackenzie Trough-Canadian Beaufort Shelf, (2) mud volcanoes, (3) central Amundsen Gulf, and (4) southwestern Banks Island.

3.2. Analytical procedure

3.2.1. *Grain-size distribution*

Sediment grain-size analyses were performed on the detrital fraction of the sediment using a Beckman Coulter LS13320 laser diffraction grain-size analyzer, which has a detection range of 0.04–2000 µm. Samples were deflocculated by successive washing with distilled water after the removal of organic matter and biogenic carbonate of the sediments with 10 mL of hydrogen peroxide (30 % H_2O_2) and 10 mL of hydrochloric acid (0.5M HCl), respectively. Biogenic silica was not removed as it appeared to be negligible (likely less than 1%, as suggested by its no detection in the bulk sediment XRD diffractograms). The grain-size distribution and statistical parameters (e.g., mean, sorting) were calculated using the moment methods in logarithmic (phi - ϕ) scale and the GRADISTAT software (Blott and Pye, 2001). Furthermore, the end-member modelling algorithm (EMMA) developed by Weltje (1997) and adapted by Dietze et al. (2012) was subsequently applied to the grain-size data in order to extract meaningful end-member (EM) grain-size distributions and estimate their proportional

192 contribution to the sediments. The cumulative explained variance (r^2) was calculated to assess the
193 minimum number of EMs needed for a good estimate of our grain-size data (Weltje, 1997; Dietze et al.,
194 2012). In general, grain-size distribution and end-member modelling analysis can be used to investigate
195 the sedimentary transfer regiweme because sediment grain-size distribution (primarily driven by
196 sedimentary processes) reflects transport conditions (e.g., Montero-Serrano et al., 2009, 2010a; Simon et
197 al., 2012; Dietze et al., 2012).

198 3.2.2. *Bulk magnetic properties*

199 Low-field magnetic susceptibility (k_{LF}) was measured on bulk sediment samples using a
200 Bartington MS2E. The k_{LF} values primarily reflect changes in the ferrimagnetic concentration (e.g.,
201 magnetite or titanomagnetite), but they are also sensitive to magnetic grain-size variations (Dunlop and
202 Özdemir, 1997). In order to explorer the possible presence of ultrafine superparamagnetic (SP) particles,
203 Frequency-dependent magnetic susceptibility was measured in some bulk sediments samples, at low-
204 (0.465 kHz; k_{lf}) and high- (4.65 kHz; k_{hf}) frequencies, on a Bartington Susceptibility Meter (model
205 MS2B) with a dual-frequency sensor (Dearing, 1999). The per sample measuring time is 10s and data
206 output is in SI units (10^{-5} SI). Each measurement was repeated at least five times and the readings were
207 averaged. The measurement of hysteresis loops and derived properties, including saturation remanence
208 (M_r), saturation magnetization (M_s), bulk coercive force (H_c), and remanent coercive force (H_{cr}) were
209 determined using an alternating gradient force magnetometer (AGM) MicroMag 2900 from Princeton
210 Measurements Corporation. The M_{rs}/M_s and H_{cr}/H_c ratios can be used as grain-size proxies (the so-called
211 Day plot) as well as to identify the magnetic domain state when the principal remanence-carrier mineral
212 is magnetite (Day et al., 1977; Dunlop, 2002; Stoner and St-Onge, 2007).

213 3.2.3. *Bulk sediment mineralogy and elemental geochemistry*

214 Before the bulk mineralogical and geochemical analysis, the sediment samples were rinsed five
215 times with distilled water after the removal of organic matter fraction with 10 mL of hydrogen peroxide

(30 % H_2O_2). Next, sediment samples were ground with a McCrone micronizing mill using 5 mL of ethanol and grinding times of 5–10 min to obtain a homogeneous powder. The slurry was oven-dried overnight at about 60°C and then slightly homogenized with an agate mortar to prevent any agglomeration of finer particles during drying. Aliquots of these sediment samples were used for bulk mineralogical and geochemical analysis.

Bulk mineral associations were studied by X-ray diffraction (XRD). The random powder samples were side-loaded into the holders and analysed on a PANalytical X'Pert Powder diffractometer. This instrument is fitted with a copper tube (Cu K-alpha = 1.54178 Å), operating at 45 kV and 40 mA and a post-diffraction graphite monochromator. Samples were scanned from 5° to 65° two-theta in steps of 0.020° two-theta and a counting time of 2 seconds per step. For the semi-quantification of the major mineralogical components, bulk sediment XRD scans were processed in the software package X'Pert High-Score Plus (PANalytical) using the Rietveld full-pattern fitting method (e.g., Young, 1993; Grunsky et al., 2013). This method permits the semi-quantification of whole-sediment mineralogy with a precision of 5–10% for phyllosilicates and 5% for non-phyllosilicates minerals. The quality of the Rietveld fitting procedure was evaluated for the R-profile and goodness-of-fit (GOF). The R-profile quantifies the difference between the observed and calculated patterns, whereas the GOF is the ratio between the R-weighted profile (RWP; best least-squares fit between observed and calculated patterns) and R-expected theoretical (Rexp; best possible value for the residual). An R-values profile between 20–30 % and a GOF of fewer than 3 are typically adequate in the Rietveld refinement of geological samples (e.g., Young, 1993). The major mineralogical components quantified by this technique are: quartz, potassium (K) feldspar (microcline + orthoclase), plagioclase feldspar (albite + anorthite), amphibole (hornblende), pyroxene (augite), magnetite, Fe-oxides (hematite + goethite), dolomite, and phyllosilicates (biotite, muscovite, illite, chlorite, and kaolinite).

A total of 14 elements (Al, Si, K, Mg, Ca, Ti, Mn, Fe, P, Sr, V, Cr, Zn, and Zr) were analysed by energy dispersive X-ray fluorescence (EDXRF) spectrometry using a PANalytical Epsilon 3-XL. Before EDXRF analysis, loss on ignition (LOI) was determined gravimetrically by heating the dried samples up to 950°C for two hours. Subsequently, samples were treated by borate fusion in an automated fusion furnace (CLAISSE® M4 Fluxer). Samples weighing ~0.6 g were mixed with ~6 g of lithium borate flux (CLAISSE, pure, 49.75% $Li_2B_4O_7$, 49.75% $LiBO_2$, 0.5% LiBr). The mixtures were melted in Pt-Au crucibles (95% Pt, 5% Au), and after fusion the melts were cast to flat disks (diameter: 32 mm; height: 3 mm) in Pt–Au moulds. Acquired XRF spectra were processed with the standardless Omnian software package (PANalytical). The resulting data are expressed as weight percent (wt.% ; Al, Si, K, Mg, Ca, Ti, Mn, Fe, P) and micrograms per gram (μg/g; V, Cr, Zn, Sr, Zr). Procedural blanks always accounted for less than 1% of the lowest concentration measured in the sediment samples. Analytical accuracy and precision were found to be better than 1–5% for major elements and 5–10 % for the other elements, as checked by an international standard (USGS SDC-1) and analysis of replicate samples. Because Al and Si are associated to clay minerals, aluminosilicates and quartz, and Ca is associated to carbonates, the ternary plot Al-Si-Ca (expressed as oxides) was used here in order to obtain a general geochemical classification of the sediments (e.g., Brumsack, 1989; Meinhardt et al., 2014). In addition, to compare the relative enrichment of redox-sensitive elements (Mn, Fe, V, Cr, Zn), we calculated enrichment factors (EF) by comparing Al-normalized metal concentrations to those of average shale (Wedepohl, 1991): $X_{EF} = [(X/Al)_{sample} / (X/Al)_{average\ shale}]$. In practical terms, EF > 3 represents a detectable authigenic enrichment of an element over average shale concentrations, whereas EF > 10 represents a moderate to strong degree of authigenic enrichment (e.g., Tribovillard et al., 2006).

In addition, in order to identify the presence of authigenic minerals (such as, carbonate, iron oxides, and greigite) within the mud volcanoes province, some bulk sediments and white crusts observed in the samples were analyzed using a JEOL 6460LV scanning electron microscope equipped with an

Energy Dispersive X-ray Spectrometer (SEM-EDS). The image and EDS analyses were obtained with a backscatter detector, an accelerating voltage of 20 kV and a spot size of 60 (probe diameter).

3.3. Statistical and spatial approach

The mineralogical and geochemical data are of a compositional nature, that is, they are vectors of non-negative values subjected to a constant-sum constraint (usually 100%). This implies that relevant information is contained in the relative magnitudes, so statistical analysis must focus on the ratios between components (Aitchison, 1986). Under this framework, a principal component analysis (PCA) was performed on the mineralogical and elemental geochemical dataset with the goal of finding elemental and mineralogical associations with similar relative variation patterns that may be interpreted from a palaeoenvironmental standpoint (e.g., von Eynatten et al., 2003; Montero-Serrano et al., 2010b, 2015; von Eynatten et al., 2016). Likewise, a fuzzy c-means clustering analysis was performed using the mineralogical dataset with the goal of ascertaining whether the differences observed between each sedimentological province are statistically valid. The results from the fuzzy c-means clustering are visualized by a silhouette plot (Kaufman and Rousseeuw, 2009), where each sediment sample is represented by a bar (silhouette width) that ranges from 0 (no similarity) to 1 (identical). Thus, the silhouette plot allows a visualization of the quality of the clustering and the distinctiveness of the sediment samples (Borcard et al., 2011). Prior to all multivariate analyses, a log-centred (clr) transform was applied to the data (Aitchison, 1990). The clr transform is derived by dividing each variable (e.g., mineral percentage, element concentration) by the geometric mean of the composition of the individual observations and then taking the logarithm. This operation removes statistical constraints on compositional variables, such as the constant-unit sum, and allows the valid application of classical (Euclidean) statistical methods to compositional data (Aitchison, 1986; 1990). All statistical calculations were conducted with “R” software using the packages “StatDA” (Reimann et al., 2008), “compositions”

(van den Boogaart and Tolosana-Delgado, 2008), “vegan” (Oksanen et al., 2015), and “cluster” (Maechler et al., 2015). Finally, the scores from the first two principal components of the log-centred data were used to produce interpolated compositional maps in ArcGIS® software. The interpolated maps were generated using the Spline with Barriers algorithm available in ArcGIS® Spatial Analyst Tools. This method of interpolation produced a smooth surface with values in the range of the scores of data points using a minimum curvature spline technique (Childs, 2004). However, the interpolated surfaces closest to the borders are biased by this method and should be interpreted with caution.

All analytical data presented are available in the supplementary material.

4. Results and Interpretations

4.1. Grain-size distribution

The mean sediment grain size (phi scale) ranges from 8.31 (clay) to 6.79 (fine silts), with minimum phi values within the southwestern Banks Island province (Figure 2A). Interestingly, although all sediment samples are poorly sorted (values of $1.25<\sigma_{\phi}<1.75$; Figure 2B) in the study area, relatively higher sorting (values up to 1.75) is found in some samples from the mud volcanoes area in the Canadian Beaufort Shelf (samples 403, 609, 709, 711, 712, 805) as well as in the southwestern Banks Island (samples 2015 and 415) (Figure 2B). In correspondence with this result, the end-member modelling analysis (EMMA) produced a three-EM model to explain more than 91% of the total variance (Figure 3A). The sediment samples are characterized by three grain classes with different grain-size distribution (Figure 3B-C): (1) the EM1 end-member (mean ~8.8 ϕ; bimodal distribution) is associated to the clay to very fine silt fraction and characterizes many samples in the shallow Canadian Beaufort Shelf; (2) the EM2 end-member (mean ~ 6.3 ϕ; bimodal distribution) is associated to the fine silt fraction, which is most of the sediments studied; and (3) the EM3 end-members (mean ~5.9 ϕ; trimodal distribution)

correspond to the medium to fine silt fraction of samples 403, 805, and 709 from the mud volcanoes in the Canadian Beaufort Shelf and 415, 312, and 315 from the southwestern Banks Island.

4.2. Magnetic properties

Hysteresis loops of representative samples are shown in Figure 4A. All hysteresis loops display saturation fields (<250 mT) and shapes suggesting the assemblage of magnetic grains is mainly dominated by magnetite. Similarly, the M_{rs}/M_s - H_{cr}/H_c crossplots or Day plot (Figure 4B) illustrate that most of the magnetic grains within the sediment samples are composed of pseudo-single domain (PSD) magnetite (Dunlop, 2002). However, some poorly sorted and coarser samples (106 and 109 from the central Amundsen Gulf; 609 and 709 from the mud volcanoes in the Canadian Beaufort Shelf; Figure 3B) show a scattered distribution on the Day plot (Figure 4B), most probably reflecting the presence of coarser magnetite grains (e.g., Lisé-Pronovost et al., 2009; Brachfeld et al., 2009). Magnetic susceptibility values range between 4.4 and 35.7 ($x10^{-5}$ SI units; Figure 5A), with maximum values recorded in samples from the southwestern Banks Island coast (samples 215 and 415), central Amundsen Gulf (sample 115) and mud volcanoes in the Canadian Beaufort Shelf (samples 400, 403, 609, 709 and 803). Differences in the frequency-dependent susceptibility for these last sediment samples are negligible (k_{lf}/k_{hf} ~ 1; Table S1), suggesting low to very low contents of superparamagnetic grains. The magnetic susceptibility, M_{rs}/M_s and H_{cr}/H_c ratios show similar distribution patterns (Figure 5), most likely suggesting that magnetic susceptibility changes are driven by magnetic grain-size variations. Interestingly, the southwestern Banks Island coast and Amundsen Gulf grains have slightly lower ratios of H_{cr}/H_c and higher ratios of M_{rs}/M_s than the Mackenzie Trough-Canadian Beaufort Shelf samples (Figure 5B-C and 12F), possibly indicating a slighter finer magnetic grain size. Similar results in magnetic mineralogy have also been reported in the sedimentary records from the Mackenzie Trough-Canadian Beaufort Shelf area (e.g., Barletta et al., 2010; Barris, 2012).

4.3. Bulk mineralogy composition

The Mackenzie Trough-Canadian Beaufort Shelf and Amundsen Gulf bulk mineralogy (Figure S1 in the auxiliary material) is dominated by quartz (28–64%), phyllosilicates (15–48%), dolomite (3–35%), Na-plagioclase (4–11%), and K-feldspar (3–10%), and by lower proportions of Fe-oxides (0.2–1.5%), calcite (<1%), magnetite (<0.7%), and pyroxene (<1.0%). Amorphous silica (e.g., diatoms) was not detected in the XRD diffractograms in the studied samples due to its low content (likely <1%). Quartz, K-feldspar, plagioclase, phylosilicates and dolomite represented more than 91% of the overall mineral concentration in the sediment samples. In order to reduce dimensionality in the data and identify mineral associations, a principal component analysis (PCA) was conducted (Figure 6A). This analysis indicates that PC-1 (65.37% of the total variance) is positively associated with dolomite and negatively associated with phyllosilicates, Fe-oxides, and magnetite, whereas PC-2 (19.54% of the total variance) is positively associated with plagioclase and quartz and negatively associated with K-feldspar as well as dolomite, magnetite, and Fe-oxides (Figure 6B). The spatial distributions of the PC-1 and PC-2 mineralogical scores (Figure 7) reveal that the southwestern Banks Island and central Amundsen Gulf provinces are relatively enriched in dolomite and K-feldspar, whereas the Mackenzie Trough-Canadian Beaufort Shelf is characterized by higher contents in phyllosilicates, Fe-oxides, and magnetite (Figure 7A). Intermediate PC-1 scores and high PC-2 scores (up to 1.4) are observed in the coarse multimodal samples from the mud volcanoes province and reflect intermediate and higher concentrations of dolomite and plagioclase-quartz, respectively (Figure 7B).

4.3. Elemental geochemistry

356 The major element composition (Figure S2 in the auxiliary material) in the Mackenzie Trough-
357 Canadian Beaufort Shelf and Amundsen Gulf sediments is dominated by Si (25–37 wt.%), Al (4–10
358 wt.%), Ti (0.2–0.5 wt.%), Ca (1–8 wt.%), Fe (2–6 wt.%), K (1–3 wt.%), Mg (0.6–5 wt.%), P (0.2–0.8
359 wt.%), and Mn (0.02–2.2 wt.%), while the minor and trace elements are dominated by V (120–325
360 µg/g), Zr (134–227 µg/g), Sr (107–209 µg/g), Zn (84–205 µg/g), and Cr (81–163 µg/g). LOI values
361 range from 3 to 17.5 wt.%.

362 The ternary plot Al_2O_3-SiO_2-CaO (Figure 8A) illustrates that the sediments from the Mackenzie
363 Trough-Canadian Beaufort Shelf are dominantly composed of detrital material similar to average shale,
364 whereas the central Amundsen Gulf and southwestern Banks Island sediments show higher detrital
365 carbonate contents (dolomite) and plot along the mixing line from average shale to the detrital carbonate
366 end-member. Some sediment samples from the mud volcanoes (samples 403, 609 and 709) and central
367 Amundsen Gulf (sample 106) are enriched in quartz (SiO_2 >45%; Figure 8A). Furthermore, Fe/Al and
368 Mn/Al display a high positive linear correlation (r=0.75; Figure 8B), indicating a geochemical
369 relationship most likely similar to Fe–Mn oxyhydroxide phases. The enrichment factors of redox-
370 sensitive elements (V, Cr, Zn) reveal modest authigenic enrichment (1 to 3) in all sedimentological
371 provinces compared to average shale values (Figure 9). Fe shows no detectable authigenic enrichment in
372 any sediment samples, whereas Mn has moderate-to-strong authigenic enrichment (EF > 5) in the central
373 Amundsen Gulf and southwestern Banks Island and modest enrichment (EF < 3) in the Mackenzie
374 Trough-Canadian Beaufort Shelf.

375 Principal component analyses based on these major, minor, and trace elements (Figure 10A)
376 reveal that the PC-1 scores (71.05% of the total variance) are positively associated with Ca-Mg-LOI and
377 negatively associated with Al-K-Ti-Fe-Cr-V-Zn-P, whereas the PC-2 scores (11.27% of the total
378 variance) are positively associated with Si-Zr-Cr-Ca-P and negatively associated with K-Fe-V-Mg-LOI
379 (Figure 10B). Importantly, Mn was omitted in the PCA because of the large influence on the

geochemical variability. The Mn surface distribution show higher concentrations in central Amundsen Gulf and southwestern Banks Island sediments compared to the Canadian Beaufort Shelf (Figure 11A). Moreover, the spatial distributions of the PC-1 and PC-2 elemental geochemical scores (Figure 11B-C) reveal similar trends as those observed in the bulk minerals (Figure 7), with large positive PC-1 scores (Ca-Mg-LOI) in the southwestern Banks Island and central Amundsen Gulf provinces and large negative PC-1 scores (Al-K-Ti-Fe-Cr-V-Zn-P) in the Mackenzie Trough-Canadian Beaufort Shelf province. Some coarse multimodal samples from the mud volcanoes province are characterized by positive PC-2 scores, which are associated with Si-Zr-Cr and Ca-P (Figure 11B).

SEM-EDS analysis performed on white crusts observed in mud volcanoes sediments (e.g., station 609; Figure S3 in the auxiliary material) reveal Ca-Mg peaks, suggesting that these white crusts most probably represent authigenic carbonate minerals (notably, low Mg-calcite and/or dolomite). In addition, authigenic iron sulfides (such as, pyrite and greigite) were not observed in the bulk sediment particles during the SEM-EDS analysis.

4.4. Relationship between grain size, bulk mineralogy, elemental geochemistry, and magnetic properties

In order to explore the relationship among the grain size and PC scores from the bulk mineralogy and elemental geochemistry, a bivariate correlation was conducted (Figure 12). Note that sediment samples from the mud volcanoes province were not plotted because they are formed by different sedimentary processes. PC-1 scores derived from bulk mineralogy and elemental geochemistry exhibit a good-to-modest negative correlation with the mean grain size on the phi-scale, respectively (Figure 12A-B). This correlation suggests that variations in the mineralogical and geochemical signatures of surface sediments from the Mackenzie Trough-Canadian Beaufort Shelf and Amundsen Gulf are not only

dominated by the relative contribution of the different sediment sources, but are also a function of grain-size sorting. In fact, a west-east trend in sediment composition and grain size may be observed in Figures 2A, 3A, 4C, 5c and 12A-C. In the Mackenzie Trough-Canadian Beaufort Shelf sediments, the phyllosilicate–Fe-oxide–magnetite (negative PC-1 scores from XRD) and Al-K-Ti-Fe-Cr-V-Zn-P (negative PC-1 from XRF) contents are highest in the clay to very fine silt fraction ($7.5<\phi<8.5$), whereas dolomite−K-feldspar (positive PC-1 scores from XRD) and Ca-Mg-LOI (positive PC-1 scores from XRF) contents are highest in the very fine to fine silt fraction ($6.5<\phi<7.5$) of the southwestern Banks Island sediments. Interestingly, there is a weak negative correlation with the mean grain size in phi units for the magnetic susceptibility (k_{lf}) (Figure 12C), suggesting that the k_{lf} variability can only partly be explained by the grain-size sorting. In general, the lowest magnetic susceptibility (k_{lf}) is recorded in the clay to very fine silt fraction, where the magnetite and Fe-oxide contents are highest (Figure 6A), with an inverse trend observed in the fine silt fraction.

To explore the relationship among the magnetic susceptibility (k_{lf}) and the mineralogical and geochemical signatures in the surface sediments, a bivariate correlation was also performed. A good positive correlation is observed between all detrital proxies used here (Figure 12D-F), suggesting that: (1) the minerals and chemical composition of detrital particles are highly intercorrelated, and thus, phyllosilicates–Fe-oxides–magnetite are associated with Al-K-Ti-Fe-Cr-V-Zn-P contents, whereas dolomite–K-feldspar are associated with Ca-Mg-LOI contents; and (2) magnetic minerals (notably, magnetite) are derived mainly from detrital sources.

Since the distribution of geochemical elements in the Canadian Beaufort Sea-Amundsen Gulf region is closely linked to the mineralogical distribution (Figure 12E), either may be used to discriminate regional groups (or provinces) with a different sedimentary composition. Consequently, we performed a fuzzy c-means clustering analysis based on four unassociated key minerals (quartz–phyllosilicates–K-

feldspar–dolomite; Figure 6A) to ascertain whether the differences between each predefined province are statistically valid. The ordination diagram and silhouette plots corroborates that sediment samples can be divided into four homogeneous clusters or sedimentary provinces (Figure 13), as indicated by their relatively high membership value (up to 0.60; Figure 13B): (1) Mackenzie Trough-Canadian Beaufort Shelf, (2) southwestern Banks Island, (3) central Amundsen Gulf, and (4) mud volcanoes.

5. Discussion

The spatial variations observed in the siliciclastic grain size, magnetic properties, mineralogical, and geochemical record from the Mackenzie Trough-Canadian Beaufort Shelf and Amundsen Gulf sediments are likely related to changes in redox conditions, surface detrital provenance, and sediment dispersal of the land-derived particles delivered by the Mackenzie River to the shelf and coastal erosion.

5.1. Sedimentary redox conditions

Given that Mn forms a highly insoluble oxyhydroxide where oxic conditions prevail (Burdige, 1993; Calvert and Pedersen, 2007), the moderate to strong degree of Mn enrichment (EF > 5) in the central Amundsen Gulf and southwestern Banks Island sediments compared to the Canadian Beaufort Shelf suggests that more oxic conditions prevail at the sediment-water interface in this area (Figure 9 and Figure 11A). In agreement with previous geochemical studies (e.g., O'Brien et al., 2006; Mucci et al., 2010; Tremblay et al., 2014), we hypothesize that these differences in oxic conditions are likely related with more turbulent mixing of the water column. Indeed, despite the pronounced stratification (Tremblay et al., 2014), strong winds in conjunction with recurrent ice-free conditions for much of the year likely led to strong vertical mixing within Amundsen Gulf. These conditions produce a well-oxygenated water column, but also promote the settling of Fe-Mn oxyhydroxide particles onto the seafloor (e.g., Macdonald and Gobeil, 2012). Conversely, on the Canadian Beaufort Shelf, the large supply of

terrigenous organic matter from the Mackenzie River keeps the oxic-anoxic boundary close to the sediment-water interface and allows the reductive remobilization and release of Fe and Mn from oxyhydroxide coatings into the uppermost sediments and overlying water column (Magen, 2007; Magen et al., 2011). Alternatively, the high Mn-enrichment factors found in the central Amundsen Gulf and southwestern Banks Island (Figure 9) may also be related to the lower detrital Al-rich minerals (Figure 8B) received in these zones as no large rivers discharge into Amundsen Gulf and only a small amount of the Mackenzie River sediment plume reaches the Gulf (e.g., Hill et al., 1991; Macdonald et al., 1998). However, as shown in Figure 9, redox-sensitive elements (Fe, V, Cr, Zn) are not authigenically enriched (EF <3), supporting the idea that predominantly oxic conditions prevail at the sediment-water interface (e.g., Magen, 2007). Accordingly, these redox-sensitive elements reveal a good association with Al, advocating a mostly detrital origin (Figure 10A).

5.2. Sedimentary provinces and sediment provenance

The spatial distribution of principal component scores, together with fuzzy c-means clustering analysis, indicates that there are four provinces with distinct sedimentary compositions within the Mackenzie Trough-Canadian Beaufort Shelf and Amundsen Gulf, as described below.

5.2.1. *Mackenzie Trough-Canadian Beaufort Shelf*

This sedimentary region is the most widespread and is characterized by mineral (phyllosilicates, Fe-oxides, magnetite) and element (Al-K-Ti-Fe-Cr-V-Zn-P) associations mainly found in the fine-grained aluminosilicate and Fe-Mn oxide fractions. The variability in detrital input delivered to the Canadian Beaufort Shelf via the Mackenzie River discharge and the subsequent hydraulic sorting most probably controls the distribution and accumulation of these minerals and elements. Note that sediment contribution to the Canadian Beaufort Sea by the Arctic Alaskan rivers and coastal erosion is relatively small compared to the Mackenzie River discharge (Hill et al., 1991). Likewise, with the exception of the

475 mud volcanoes areas, the PC scores from both bulk mineralogy and elemental geochemistry (Figures 7
476 and 11B-C), as well as the Al-Si-Ca relationship (Figure 8A), exhibit a homogeneous sedimentary
477 composition within this province. This homogeneity suggests a common detrital particle provenance and
478 supports the notion that the Mackenzie River sediment plume has a wide easterly propagation, thus
479 influencing modern sedimentation in the entire Canadian Beaufort Shelf area (e.g., Hill et al.,
480 1991;Carmack and Macdonald, 2002; Richerol et al., 2008b).

481 The overall mineralogical and geochemical signatures characterizing this province, point to a
482 detrital input from a more aluminosiliciclastic-carbonate sedimentary source such as the Cambrian to
483 Cretaceous shales, sandstones and limestone cropping out in the Interior Platform. This assumption is in
484 agreement with the Sr isotope composition of suspended sediments from the Mackenzie basin (Millot et
485 al., 2003), suggesting that the Mackenzie River system is mostly dominated by the tributaries of the
486 Interior Plain, with the northern Rockies and Mackenzie Mountains as secondary sources. In addition,
487 compared to the rivers of the Mackenzie and Rocky Mountains, those of the interior plains also supply
488 large amounts of terrestrial organic matter to the Canadian Beaufort Shelf (Millot et al., 2003), almost all
489 of which (~97%) is deposited on the inner to middle shelf (Macdonald et al., 1998; O'Brien et al., 2006).
490 Accordingly, the slightly lower magnetic susceptibility (k_{lf}) values in this province, where the iron-
491 bearing mineral (magnetite and Fe-oxides) contents are highest, may be accounted for by a dilution
492 effect from a high organic-matter supply (e.g., Bloemendal et al., 1992). The large amounts of
493 terrigenous organic material deposited on the Canadian Beaufort Shelf compared to Amundsen Gulf
494 (e.g., Macdonald et al., 1998; Magen et al., 2010), lead to organic matter diluting the highly magnetic
495 fine-grained material and, therefore, producing low magnetic susceptibility (k_{lf}) values.

496 5.2.2. *Southwestern Banks Island*

497 This province is characterized mainly by the association of dolomite–K-feldspar and Ca-Mg-LOI
498 and, to a lesser extent, by phyllosilicates, Fe-oxides and Mn (Figures 7 and 11A-C). Likewise, fine silt

499 contents are higher in this province compared to the Mackenzie Trough-Canadian Beaufort Shelf area
500 (Figures 2A and 3C). Since biogenic carbonates are only of subordinate importance (calcite <1%),
501 detrital carbonate (dolomite) is the main host mineral for Ca-Mg-LOI (Figures 7 and 11). In agreement
502 with petrographic and bulk mineralogy studies performed around Banks Island (e.g., Bader and Henry,
503 1961; Bischof et al., 1996; Vogt, 1997), we hypothesize that most of the fine silt detrital sediments in
504 this province are mainly supplied from coastal cliff erosion of fine-grained Pleistocene carbonate-rich
505 glacial tills and clastic sedimentary rocks cropping out on southwestern Banks Island. In fact, much of
506 the coastline along southwestern Banks Island and Amundsen Gulf is vulnerable to coastal erosion
507 (O'Brien et al., 2006). According to Belliveau (2007), the summer melting of ground ice on the
508 southwestern coast of Banks Island generally leads to slumping along coastal cliffs, which not only
509 creates large erosional areas, but also increases the amount of fine-grained sediments available that can
510 reach the coastline, especially during the open-water season (June-September) when southeast winds and
511 onshore storm winds predominate.

512 Compared to the Mackenzie Trough-Canadian Beaufort Shelf province, this zone has a less-
513 extended modern detrital contribution to the eastern part of Amundsen Gulf (Figures 7A and 11B). Note,
514 however, that from a more regional perspective and based on the geochemical fingerprint of entrained
515 Fe-oxide mineral grains in Arctic Ocean sea ice, Darby (2003) suggests that the Banks Island shelf is the
516 most important source of sediment accumulated from ice floes in the Beaufort Sea, northern Chukchi
517 Sea, and the Chukchi Borderland area. Indeed, easterly winds dominate the ice-cover dynamics in the
518 Canadian Beaufort Sea region (Hill et al., 1991) and promotes a recurrent polynya (known as the Cape
519 Bathurst Polynya; Arrigo and van Dijken, 2004) on the southwestern coast of Banks Island (Figure 1). In
520 this shallow, ice-free area, stronger winds in fall and winter induce turbulent mixing of the water
521 column, leading to both a more oxygenated water column and the recurrent incorporation of shelf
522 sediments into the sea ice (a process known as suspension freezing; Reimnitz et al., 1993). These sea ice

and ice floes are subsequently transported westwards of the area via surface currents and the clockwise BG current system (Darby, 2003).

5.2.3. *Central Amundsen Gulf*

This province represents a transitional zone between the Mackenzie Trough-Canadian Beaufort Shelf and southwestern Banks Island sedimentary provinces and is characterized by intermediate phyllosilicate-magnetite-dolomite-K-feldspar and Al-K-Ti-Fe-Mn-V-Zn-Sr-Ca-Mg-LOI contents (Figures 7 and 11). Similarly to southwestern Banks Island sediments, fine silt contents are also higher in this province compared to the Mackenzie Trough-Canadian Beaufort Shelf area (Figures 2A and 3A). Thus, this zone consists mainly of minerals and elements resulting from a mixture of (1) the aluminosiliciclastic and iron-bearing material likely derived from the Mackenzie River discharge and (2) detrital carbonate and K-feldspar derived from coastal erosion of southwestern Banks Island. Indeed, re-suspended shelf sediment and sediment from the Mackenzie River discharge may reach Amundsen Gulf in the summer when northwesterlies dominate (O'Brien et al., 2006). In contrast, because southwestern Banks Island is not influenced by significant river discharges, coastal cliff erosion plays a more important role in sediment supply and transport to the central Amundsen Gulf (Belliveau, 2007). Alternatively, we cannot rule out that other secondary source rivers, such as the Horton and Hornaday rivers (Figure 1), might also reach the Amundsen Gulf during break-up in the spring. Furthermore, because the drainage basin of these rivers is covered by Palaeozoic sedimentary rocks as well as fine-grained Pleistocene potassium-rich glacial till resulting from the glacial erosion of Precambrian Canadian Shield rocks (e.g., Padgham and Fyson, 1992), they may also supply quartz and K-feldspar minerals to the Gulf.

5.2.4. *Mud volcanoes*

This province is characterized by poorly sorted medium to fine silt sediments (Figures 2B and 3C) with high quartz-plagioclase, authigenic carbonate (low Mg-calcite and/or dolomite; Figures 7 and

S3) and Si-Zr (Figure 11) contents, as well as high magnetic susceptibility values (Figure 5A). As no large rivers discharge to the east Mackenzie River (R-ArcticNet database) and coastal erosion is only an important local sediment supply near the shoreline in the Canadian Beaufort Shelf (Carmack and Macdonald, 2002), we hypothesize that detrital sediments supply within these specific areas are driven by the mud volcanoes activity. Based on seismic stratigraphy studies performed along the eastern Canadian Beaufort Shelf (Blasco et al., 1990; Hill et al., 1991; Batchelor et al., 2013) and submarine mud volcanoes distribution (Blasco et al., 2013), we presume that the detrital sediment in these areas derived from the subsurface sediment remobilisation of the fine-grained Pleistocene quartz-rich glacial tills deposited in the Shelf following mud migration towards the surface. Indeed, fluidized/gasified sediment eruptions associated with the mud volcanoes activity promote the remobilization and transport to the seafloor of the sediments accumulated in the subsurface (Paull et al., 2007; 2015). This interpretation is in agreement with previous studies on the mud volcanoes from the Canadian Beaufort Shelf (e.g., Paull et al., 2007; Blasco et al., 2013; Paull et al., 2015) that suggest that the crest sediments are significantly older than the moat sediments and they almost certainly pre-date the marine transgression (Hill et al., 1993). In addition, the mud volcanoes are also most likely responsible for the higher magnetic susceptibility values in these areas. Lower ratios of Mrs/Ms and higher ratios of Hcr/Hc suggest that mud volcanoes sediments are dominated by coarser magnetite grains (Figure 4), which are responsible for the increase in magnetic susceptibility recorded within this province. This is consistent with the remobilization of fine till material towards the surface by the mud volcanos activity.

On the other hand, the high authigenic carbonate contents observed in this province may be related with the gas hydrate decomposition (Moore et al., 2004; Yang et al., 2014). In fact, ascending venting methane derived from the gas hydrate decomposition come in contact with seawater sulfate near the seafloor, where an anaerobic oxidation of methane takes place, favoring the authigenic carbonate precipitation (which may include calcite, dolomite, and/or aragonite). This environmental process has

been proposed to operate in different mud volcanoes settings from Fram Strait (Ambrose et al., 2015), South China Sea (Yang et al., 2014), Niger deep-sea fan (Bayon et al., 2007), and Mediterranean (Pancost et al., 2001), among others.

To summarize, the spatial trends of our mineralogical, geochemical, and magnetic data, together with the fuzzy c-means clustering analysis, suggest that: (1) the Mackenzie River discharge is the main contributor of terrigenous sediments in the entire Canadian Beaufort Shelf, (2) southwestern Banks Island represents a secondary source of sediments in the central Amundsen Gulf, (3) sediments from the central Amundsen Gulf represent a mix of sediments derived from both the Mackenzie River discharge and coastal erosion of southwestern Banks Island, and (4) the Canadian Beaufort Shelf area is preferentially influenced by mud volcanoes activity (see summary in Figure 14).

5.3. Comparison to other circum-Arctic regions — mineralogical clues

Continents surrounding the Arctic Ocean comprise bedrock/soils characterized by different petrographic signatures (e.g., Vogt, 1997; Stein, 2008; Harrison et al., 2008; Bazhenova, 2012; Fagel et al., 2014; Linsen et al., 2014). Consequently, as suggested by Vogt (1997), surface sediments from circum-Arctic source areas may be characterized by very specific K-feldspar/plagioclase (Kfs/Plg) and quartz/(K-feldspar + plagioclase) (Qz/Fsp) ratios. To verify this notion, we compared our bulk mineralogical data with other circum-Arctic regions (Figure 15), notably with surface marine sediments from the Eurasian shelf (Stein, 2008; Bazhenova, 2012), Bering Strait (Linsen et al., 2014), as well as with continental sediments from the northern Yukon Territory, Tuktoyaktuk Peninsula, Cape Bathurst, and Banks Island (Vogt, 1997). Our findings indicate that sediments from the Mackenzie Trough-Canadian Beaufort Shelf, Amundsen Gulf, and Banks Island have higher Qz/Fsp (2 to 4) and Kfs/Plg (>0.7) ratios compared to Eurasian sediments (Figure 15). In the study area, quartz and K-feldspar are mainly supplied by the Mackenzie River discharge (which drain large sedimentary platforms) and by

coastal erosion of the Pleistocene potassium- and carbonate-rich glacial till cropping out on southwestern Banks Island. In contrast, rivers from the Eurasian margin drain large basaltic provinces that can supply high amounts of plagioclase (Stein, 2008). Plagioclase weathers much faster than K-feldspar as silicate weathering preferentially attacks Na- and Ca-rich minerals (White et al., 2001). In glacial environments, this implies that mechanical comminution of plagioclase is more effective than K-feldspar during the initial stages of feldspar weathering (e.g., von Eynatten et al., 2016). As a result, plagioclase is enriched over K-feldspar in the Eurasian shelf sediments compared to the Canadian Beaufort Shelf and Amundsen Gulf, and thus yields sediments with lower Qz/Fsp (0.2-1) and Kfs/Plg (0.2-0.7) ratios (Figure 15). On the other hand, sediment samples from the mud volcanoes province display higher Qz/Fsp (>3) ratios similar to the glacial tills cropping out along the northern Yukon Territory (VH83-014), Tuktoyaktuk Peninsula (VH85-045), and Cape Bathurst (VH85-006), suggesting a common detrital origin for these sediments, which likely originate from the glacial activity of the Laurentide Ice Sheet. These also support our interpretation that the mud volcanoes province are composed of glacial tills that have been remobilized from the subsurface of the Canadian Beaufort Shelf (see section 5.2.4.). Finally, little difference is observed between surface sediments from the Bering Strait and Eurasian sediments (Figure 15) because Bering Strait sediments also contain significant amounts of plagioclase that mainly originated from the Anadyr River drainage basin, where volcanic, granitic, and granodiorite rocks crop out (e.g., Linsen et al., 2014).

6. Conclusions

The spatial variability of continental input, surface currents, and redox conditions within the Mackenzie-Beaufort Sea Slope and Amundsen Gulf was investigated through analyses of the grain size,

magnetic properties, and the mineralogical and geochemical composition of 34 surface sediment samples. The results of this research yield the following generalizations and conclusions:

1. The relative enrichment in redox-sensitive elements (Mn, Fe, V, Cr, Zn) suggests that modern sedimentary deposition within the Mackenzie-Beaufort Sea Slope and Amundsen Gulf took place under oxic bottom-water conditions;
2. Strong winds together with recurrent ice-free conditions for much of the year appear to be a plausible scenario for explaining the well-oxygenated water column and, therefore, the high Mn-enrichment factors observed in the Amundsen Gulf compared to the Canadian Beaufort Shelf;
3. The mineralogical, geochemical, and magnetic signatures of surface sediments allowed the identification of four provinces with distinct sedimentary compositions: (1) the Mackenzie Trough-Canadian Beaufort Shelf, characterized by minerals (phyllosilicates, Fe-oxides, magnetite) and elements (Al-K-Ti-Fe-Cr-V-Zn-P) derived mainly from the Mackenzie River discharges; (2) southwestern Banks Island, characterized by the association of dolomite–K-feldspar and Ca-Mg-LOI mainly supplied from coastal cliff erosion of Pleistocene potassium- and carbonate-rich glacial tills as well as clastic sedimentary rocks cropping out on the island; (3) the central Amundsen Gulf, which represents a transitional zone typified by intermediate phyllosilicates–magnetite–K-feldspar–dolomite and Al-K-Ti-Fe-Mn-V-Zn-Sr-Ca-Mg-LOI contents resulting from a detrital mix between the Mackenzie River discharges and coastal erosion of southwestern Banks Island; and (4) the mud volcanoes distinguished by the association quartz-plagioclase-authigenic carbonate and Si-Zr contents, as well as high magnetic susceptibility values resulting from the remobilization of glacial tills deposited in the subsurface of the Canadian Beaufort Shelf.

4. Our mineralogical data corroborate that K-feldspar/plagioclase and quartz/(K-feldspar+plagioclase) ratios (Vogt, 1997), together with detrital carbonate (dolomite), can be successfully used to track changes in terrigenous sediment input from the Canadian Beaufort Sea, Eurasian shelf, and Bering Strait.

Taken as a whole, our data provide a baseline for future studies using the mineralogical, geochemical, and magnetic signatures of sediment cores from the Mackenzie-Beaufort Sea Slope and Amundsen Gulf in order to reconstruct and document past variations in continental inputs and sediment dispersal related to climate changes.

Acknowledgements

This research is a contribution to the Canadian Arctic Shelf Exchange Study (CASES) program and was funded by the Natural Sciences and Engineering Research Council of Canada (NSERC) through Discovery Grants and FQRNT "*Nouveau chercheur*" grants to J-C Montero-Serrano, G. St-Onge and A. Rochon, as well as through Ship Time support for several expeditions (J-C Montero-Serrano, G. St-Onge and A. Rochon). We also acknowledge the financial support of the Canadian Foundation for Innovation (CFI) and Canada Economic Development for Quebec Regions (CED) for the acquisitions of the PANalytical X-ray diffractometer (X'Pert Powder) and X-ray fluorescence (Epsilon 3-XL), respectively. We also thank Quentin Beauvais, Marie-Pier St-Onge, Elissa Barris, Julie Velle, and Claude Belzile from UQAR-ISMER for their technical support and advice. Finally, we thank Christine Laurin for reviewing the grammar and Stefanie Brachfeld and an anonymous reviewer for their constructive comments that helped improve the manuscript.

References

663 Aagaard, K., 1984. The Alaskan Beaufort Sea: Ecosystems and Environments (eds P.W. Barnes, D.M.
664 Schell, & E. Reimnitz), Academic Press, Inc., 47-71.
665 Aitchison, J., 1990. Relative variation diagrams for describing patterns of compositional variability.
666 Mathematical Geology 22, 487–511. doi:10.1007/BF00890330
667 Aitchison, J., 1986. The Statistical Analysis of Compositional Data. Monographs on Statistics and
668 Applied Probability. Chapman & Hall Ltd., London (UK) (Reprinted in 2003 with additional
669 material by The Blackburn Press).
670 Arrigo, K.R., van Dijken, G.L., 2004. Annual cycles of sea ice and phytoplankton in Cape Bathurst
671 polynya, southeastern Beaufort Sea, Canadian Arctic. Geophysical Research Letters 31, 2–5.
672 doi:10.1029/2003GL018978
673 Asahara, Y., Takeuchi, F., Nagashima, K., Harada, N., Yamamoto, K., Oguri, K., Tadai, O., 2012.
674 Provenance of terrigenous detritus of the surface sediments in the Bering and Chukchi Seas as
675 derived from Sr and Nd isotopes: Implications for recent climate change in the Arctic regions.
676 Deep-Sea Research Part II: Topical Studies in Oceanography 61-64, 155–171.
677 doi:10.1016/j.dsr2.2011.12.004
678 Bader, R.G., Henry, V.J., 1961. Marine sediments of Prince of Wales Strait and Amundsen Gulf, West
679 Canadian Arctic. Compilation of articles published in the “Journal of marine research” 20 pp.
680 Barber, D.G., Hanesiak, J.M., 2004. Meteorological forcing of sea ice concentrations in the southern
681 Beaufort Sea over the period 1979 to 2000. Journal of Geophysical Research C: Oceans 109, 1–16.
682 doi:10.1029/2003JC002027
683 Barletta, F., St-Onge, G., Channell, J.E.T., Rochon, A., 2010. Dating of Holocene western Canadian
684 Arctic sediments by matching paleomagnetic secular variation to a geomagnetic field model.
685 Quaternary Science Reviews 29, 2315–2324. doi:10.1016/j.quascirev.2010.05.035
686 Barletta, F., St-Onge, G., Channell, J.E.T., Rochon, A., Polyak, L., Darby, D., 2008. High-resolution

687 paleomagnetic secular variation and relative paleointensity records from the western Canadian
688 Arctic: implication for Holocene stratigraphy and geomagnetic field behaviour. Canadian Journal of
689 Earth Sciences 45, 1265–1281. doi:10.1139/E08-039
690 Batchelor, C.L., Dowdeswell, J.A., Pietras, J.T., 2013. Seismic stratigraphy, sedimentary architecture
691 and palaeo-glaciology of the Mackenzie Trough: Evidence for two Quaternary ice advances and
692 limited fan development on the western Canadian Beaufort Sea margin. Quaternary Science
693 Reviews 65, 73–87. doi:10.1016/j.quascirev.2013.01.021
694 Bayon, G., Pierre, C., Etoubleau, J., Voisset, M., Cauquil, E., Marsset, T., Sultan, N., Le Drezen, E.,
695 Fouquet, Y., 2007. Sr/Ca and Mg/Ca ratios in Niger Delta sediments: Implications for authigenic
696 carbonate genesis in cold seep environments. Marine Geology 241, 93–109.
697 doi:10.1016/j.margeo.2007.03.007
698 Bazhenova, E., 2012. Reconstruction of late Quaternary sedimentary environments at the southern
699 Mendeleev Ridge (Arctic Ocean). Dissertation (PhD) Thesis, University of Bremen, Bremen,
700 urn:nbn:de:gbv:46-00102884-17, 83 pp.
701 Belliveau, K.D., 2007. Coastal Geomorphology of Southwest Banks Island, Northwest Territories:
702 Historical and Recent Shoreline Changes and Implications for the Future. ProQuest.
703 Bennett, R., Rochon, A., Schell, T., Bartlett, J., Blasco, S., Hughes-clarke, J., Scott, D., Macdonald, A.,
704 Rainey, W., 2008. Cruise Report Amundsen 2004-804 : Beaufort Sea / Amundsen Open File 5798
705 Geological Survey of Canada.
706 Bischof, J., Clark, D.L., Vincent, J.-S., 1996. Origin of ice-rafted debris: Pleistocene paleoceanography
707 in the western Arctic Ocean. Paleoceanography 11, 743. doi:10.1029/96PA02557
708 Bischof, J.F., Darby, D. a, 1999. Quaternary ice transport in the Canadian Arctic and extent of Late
709 Wisconsinan Glaciation in the Queen Elizabeth Islands. Canadian Journal of Earth Sciences 36,
710 2007–2022. doi:10.1139/e99-096

711 Blasco, S., Bennett, R., Brent, T., Burton, M., Campbell, P., Carr, E., Covill, R., Dallimore, S., Davies,
712 E., Hughes-Clarke, J., Issler, D., Leonard, L., MacKillop, K., Mazzotti, S., Patton, E., Rogers, G.,
713 Shearer, J., White, M., 2013. 2010 state of knowledge: Beaufort Sea seabed geohazards associated
714 with offshore hydrocarbon development. doi:10.4095/292616
715 Blasco, S.M., Fortin, G., Hill, P.R., O'Connor, M.J., Brigham-Grette, J., 1990. The late Neogene and
716 Quaternary stratigraphy of the Canadian Beaufort continental shelf. The Geology of North America
717 50, 491–502.
718 Bloemendal, J., King, J.W., Hall, F.R., Doh, S.-J., 1992. Rock magnetism of Late Neogene and
719 Pleistocene deep-sea sediments: Relationship to sediment source, diagenetic processes, and
720 sediment lithology. Journal of Geophysical Research: Solid Earth 97, 4361–4375.
721 Blott, S.J., Pye, K., 2001. Technical Communication Gradistat : a Grain Size Distribution and Statistics
722 Package for the Analysis of Unconsolidated Sediments 1248, 1237–1248.
723 Borcard, D., Gillet, F., Legendre, P., 2011. Numerical Ecology with R. Springer, New York, USA. 306
724 pp.
725 Bornhold, B.D., 1975. Suspended matter in the southern Beaufort Sea. Beaufort Sea Project. Technical
726 Report No. 25b, Department of the Environment, Victoria, British Columbia, 34 pp.
727 Brachfeld, S., Barletta, F., St-Onge, G., Polyak, L., Darby, D., 2009. Environmental magnetic record of
728 Holocene climate along the Alaska Chukchi Margin. Global and Planetary Change 68, 100–114.
729 Bringué, M., Rochon, A., 2012. Late Holocene paleoceanography and climate variability over the
730 Mackenzie Slope (Beaufort Sea, Canadian Arctic). Marine Geology 291–294, 83–96.
731 doi:http://dx.doi.org/10.1016/j.margeo.2011.11.004
732 Brumsack, H.J., 1989. Geochemistry of recent TOC-rich sediments from the Gulf of California and the
733 Black Sea. Geologische Rundschau 78, 851–882. doi:10.1007/BF01829327
734 Burdige, D.J., 1993. The biogeochemistry of manganese and iron reduction in marine sediments. Earth-

735 Science Reviews 35, 249–284. doi:http://dx.doi.org/10.1016/0012-8252(93)90040-E
736 Calvert, S.E., Pedersen, T.F., 2007. Chapter Fourteen Elemental Proxies for Palaeoclimatic and
737 Palaeoceanographic Variability in Marine Sediments: Interpretation and Application, in: Hillaire–
738 Marcel, C., Vernal, A. De (Eds.), Proxies in Late Cenozoic Paleoceanography, Developments in
739 Marine Geology. Elsevier, pp. 567–644. doi:http://dx.doi.org/10.1016/S1572-5480(07)01019-6
740 Carmack, E.C., Macdonald, R.W., 2002. Oceanography of the Canadian shelf of the Beaufort Sea: A
741 setting for marine life. Arctic 55, 29–45. doi:10.1126/science.100.2596.291
742 Carson, M.A., Jasper, J.N., Conly, P.M., 1998. Magnitude and sources of sediment input to the
743 Mackenzie Delta, Northwest Territories, 1974-94. Arctic 51, 116–124.
744 Childs, C., 2004. Interpolating surfaces in ArcGIS spatial analyst. ArcUser, July-September 3235.
745 Darby, D. a, Ortiz, J.D., Grosch, C.E., Lund, S.P., 2012. 1,500-year cycle in the Arctic Oscillation
746 identified in Holocene Arctic sea-ice drift. Nature Geoscience 5, 897–900. doi:10.1038/ngeo1629
747 Darby, D. a., 2003. Sources of sediment found in sea ice from the western Arctic Ocean, new insights
748 into processes of entrainment and drift patterns. Journal of Geophysical Research 108, 1–10.
749 doi:10.1029/2002JC001350
750 Darby, D., Bischof, J., Cutter, G., Vernal, A., Hillaire-Marcel, C., Dwyer, G., McManus, J., Osterman,
751 L., Polyak, L., Poore, R., 2001. New record shows pronounced changes in Arctic Ocean circulation
752 and climate. Eos, Transactions American Geophysical Union 82, 601–607.
753 Darby, D.A., Myers, W.B., Jakobsson, M., Rigor, I., 2011. Modern dirty sea ice characteristics and
754 sources: The role of anchor ice. Journal of Geophysical Research: Oceans 116, 1–18.
755 doi:10.1029/2010JC006675
756 Darby, D.A., Polyak, L., Bauch, H.A., 2006. Past glacial and interglacial conditions in the Arctic Ocean
757 and marginal seas - a review. Progress in Oceanography 71, 129–144.
758 doi:10.1016/j.pocean.2006.09.009

759 Davidson, S., Lank, K., De Margerie, S., 1988. Sediment transport in the Mackenzie River plume. ASA
760 Consulting Limited.
761 Day, R., Fuller, M., Schmidt, V.A., 1977. Hysteresis properties of titanomagnetites: grain-size and
762 compositional dependence. Physics of the Earth and Planetary Interiors 13, 260–267.
763 Dearing, J.A., 1999. Environmental Magnetic Susceptibility: Using the Bartington MS2 System. Chi
764 Pub., Kenilworth.
765 Dietze, E., Hartmann, K., Diekmann, B., IJmker, J., Lehmkuhl, F., Opitz, S., Stauch, G., Wünnemann,
766 B., Borchers, A., 2012. An end-member algorithm for deciphering modern detrital processes from
767 lake sediments of Lake Donggi Cona, NE Tibetan Plateau, China. Sedimentary Geology 243-244,
768 169–180. doi:10.1016/j.sedgeo.2011.09.014
769 Dunlop, D.J., 2002. Theory and application of the Day plot (Mrs/Ms versus Hcr/Hc) 1. Theoretical
770 curves and tests using titanomagnetite data. Journal of Geophysical Research: Solid Earth 107.
771 Dunlop, D.J., Özdemir, Ö., 1997. Rock Magnetism: Fundamentals and Frontiers. Cambridge University
772 Press, Cambridge, U.K.
773 Dunlop D.J., 1973. Superparamagnetic and single-domain threshold sizes in magnetite. Journal of
774 Geophysical Research 78, 1780-1793.
775 Durantou, L., Rochon, A., Ledu, D., Massé, G., Schmidt, S., Babin, M., 2012. Quantitative
776 reconstruction of sea-surface conditions over the last 150 yr in the Beaufort Sea based on
777 dinoflagellate cyst assemblages: The role of large-scale atmospheric circulation patterns.
778 Biogeosciences 9, 5391–5406. doi:10.5194/bg-9-5391-2012
779 Fagel, N., Not, C., Gueibe, J., Mattielli, N., Bazhenova, E., 2014. Late Quaternary evolution of sediment
780 provenances in the Central Arctic Ocean: Mineral assemblage, trace element composition and Nd
781 and Pb isotope fingerprints of detrital fraction from the Northern Mendeleev Ridge. Quaternary
782 Science Reviews 92, 140–154. doi:10.1016/j.quascirev.2013.12.011

783 Forest, A., Sampei, M., Makabe, R., Sasaki, H., Barber, D.G., Gratton, Y., Wassmann, P., Fortier, L.,
784 2008. The annual cycle of particulate organic carbon export in Franklin Bay (Canadian Arctic):
785 Environmental control and food web implications. Journal of Geophysical Research: Oceans 113,
786 n/a–n/a. doi:10.1029/2007JC004262
787 Galley, R.J., Key, E., Barber, D.G., Hwang, B.J., Ehn, J.K., 2008. Spatial and temporal variability of sea
788 ice in the southern Beaufort Sea and Amundsen Gulf: 1980–2004. Journal of Geophysical Research:
789 Oceans 113, n/a–n/a. doi:10.1029/2007JC004553
790 Giovando,L.F., Herlinveaux, R.H., 1981. Discussion of Factors Influencing Dispersion of Pollutants in
791 the Beaufort Sea.
792 Grunsky, E.C., Drew, L.J., Woodruff, L.G., Friske, P.W.B., Sutphin, D.M., 2013. Statistical variability
793 of the geochemistry and mineralogy of soils in the Maritime Provinces of Canada and part of the
794 Northeast United States. Geochemistry: Exploration, Environment, Analysis 13(4), 249.
795 Harrison, J.C., St-Onge, M.R., Petrov, O. V, Strelnikov, S.I., Lopatin, B.G., Wilson, F.H., Tella, S., Paul,
796 D., Lynds, T., Shokalsky, S.P., Hults, C.K., Bergman, S., Jepsen, H.F., Solli, A., 2011. Geological
797 map of the Arctic, Geological Survey of Canada Open File 5816. doi:10.4095/287868
798 Harrison, J.C., St-Onge, M.R., Petrov, O., Strelnikov, S., Lopatin, B.G., Wilson, F., Tella, S., Paul, D.,
799 Lynds, T., Shokalsky, S., others, 2008. Geological map of the Arctic.
800 Hill, P.R., Blasco, S.M., Harper, J.R., Fissel, D.B., Bornhold, D., Atlantic, T., Centre, G., Pelletier, B.R.,
801 1991. Sedimentation on the Canadian Beaufort Shelf. Continental Shelf Research 11, 821–842.
802 doi:10.1016/0278-4343(91)90081-G
803 Hill, P.R., Héquette, A., Ruz, M.-H., 1993. Holocene sea-level history of the Canadian Beaufort shelf.
804 Canadian Journal of Earth Sciences 30, 103–108. doi:10.1139/e93-009
805 Hill, P.R., Lewis, C.P., Desmarais, S., Kauppaymuthoo, V., Rais, H., 2001. The Mackenzie Delta:
806 sedimentary processes and facies of a high-latitude, fine-grained delta. Sedimentology 48, 1047–

1078. doi:10.1046/j.1365-3091.2001.00408.x

Holmes, R.M., McClelland, J.W., Peterson, B.J., Shiklomanov, I. a, Shiklomanov, A.I., Zhulidov, A. V, Gordeev, V. V, Bobrovitskaya, N.N., 2002. A circumpolar perspective on fluvial sediment flux to the Arctic ocean. Global Biogeochemical Cycles 16, 14–45. doi:10.1029/2001GB001849

Kaufman, L., Rousseeuw, P.J., 2009. Finding groups in data: an introduction to cluster analysis. John Wiley & Sons.

Kwok, R., Cunningham, G.F., Wensnahan, M., Rigor, I., Zwally, H.J., Yi, D., 2009. Thinning and volume loss of the Arctic Ocean sea ice cover: 2003–2008. Journal of Geophysical Research: Oceans 114, n/a–n/a. doi:10.1029/2009JC005312

Lammers, R.B., Shiklomanov, A.I., Vörösmarty, C.J., Fekete, B.M., Peterson, B.J., 2001. Assessment of contemporary Arctic river runoff based on observational discharge records. Journal of Geophysical Research 106, 3321. doi:10.1029/2000JD900444

Lanos, R., 2009. Circulation régionale, masses d'eau, cycles d'évolution et transports entre la mer de Beaufort et le golfe d'Amundsen. PhD Thesis, Université du Québec, Institut national de la recherche scientifique, Doctorat en sciences de l'eau, 274 p.

Linsen, D., Xuefa, S.H.I., Yanguang, L.I.U., Xisheng, F., Zhihua, C., Chunjuan, W., Jianjun, Z.O.U., Yuanhui, H., 2014. Mineralogical study of surface sediments in the western Arctic Ocean and their implications for material sources. Advances in Polar Science 25, 192–203. doi:10.13679/j.advps.2014.3.00192

Lisé-Pronovost, A., St-Onge, G., Brachfeld, S., Barletta, F., Darby, D., 2009. Paleomagnetic constraints on the Holocene stratigraphy of the Arctic Alaskan margin. Global and Planetary Change 68, 85–99. doi:10.1016/j.gloplacha.2009.03.015

Macdonald, R.W., Gobeil, C., 2012. Manganese Sources and Sinks in the Arctic Ocean with Reference to Periodic Enrichments in Basin Sediments. Aquatic Geochemistry 18, 565–591.

831 doi:10.1007/s10498-011-9149-9
832 Macdonald, R.W., Harner, T., Fyfe, J., 2005. Recent climate change in the Arctic and its impact on
833 contaminant pathways and interpretation of temporal trend data. Science of The Total Environment
834 342, 5–86. doi:http://dx.doi.org/10.1016/j.scitotenv.2004.12.059
835 Macdonald, R.W., Paton, D.W., Carmack, E.C., Omstedt, A., 1995. The freshwater budget and under-ice
836 spreading of Mackenzie River water in the Canadian Beaufort Sea based on salinity and 18O/16O
837 measurements in water and ice. Journal of Geophysical Research: Oceans 100, 895–919.
838 doi:10.1029/94JC02700
839 Macdonald, R.W., Solomon, S.M., Cranston, R.E., Welch, H.E., Yunker, M.B., Gobeil, C., 1998. A
840 sediment and organic carbon budget for the Canadian Beaufort Shelf. Marine Geology 144, 255–
841 273. doi:http://dx.doi.org/10.1016/S0025-3227(97)00106-0
842 MacNeil, M.R., Garrett, J.R., 1975. Open water surface currents Beaufort Sea Project.
843 Maechler, M., Rousseeuw, P., Struyf, A., Hubert, M., Hornik, K., 2015. cluster: Cluster Analysis Basics
844 and Extensions, 2015. R package version 1.
845 Magen, C., 2007. Origin, sedimentation and diagenesis of organic matter in coastal sediments of the
846 southern Beaufort Sea region, Canadian Arctic. PhD thesis, McGill University, Montreal, 130 pp.
847 Magen, C., Mucci, A., Sundby, B., 2011. Reduction Rates of Sedimentary Mn and Fe Oxides: An
848 Incubation Experiment with Arctic Ocean Sediments. Aquatic Geochemistry 17, 629–643.
849 doi:10.1007/s10498-010-9117-9
850 Magen, C., Chaillou, G., Crowe, S.A., Mucci, A., Sundby. B., Gao, A.G., Makabe, R., Sasaki, H., 2010.
851 Origin and fate of particulate organic matter in the southern Beaufort Sea—Amundsen Gulf region,
852 Canadian Arctic. Estuarine, Coastal and Shelf Science 86(1), 31-41.
853 Meinhardt, A.K., März, C., Stein, R., Brumsack, H.J., 2014. Regional variations in sediment
854 geochemistry on a transect across the Mendeleev Ridge (Arctic Ocean). Chemical Geology 369, 1–

855 11. doi:10.1016/j.chemgeo.2014.01.011
856 Millot, R., Gaillardet, J., Dupré, B., Allégre, C.J., 2003. Northern latitude chemical weathering rates:
857 Clues from the Mackenzie River Basin, Canada. Geochimica et Cosmochimica Acta 67, 1305–
858 1329. doi:10.1016/S0016-7037(02)01207-3
859 Montero-Serrano, J.C., Bout-Roumazeilles, V., Sionneau, T., Tribovillard, N., Bory, A., Flower, B.P.,
860 Riboulleau, A., Martinez, P., Billy, I., 2010a. Changes in precipitation regimes over North America
861 during the Holocene as recorded by mineralogy and geochemistry of Gulf of Mexico sediments.
862 Global and Planetary Change 74, 132–143.
863 Montero-Serrano, J.C., Bout-Roumazeilles, V., Tribovillard, N., Sionneau, T., Riboulleau, A., Bory, A.,
864 Flower, B., 2009. Sedimentary evidence of deglacial megafloods in the northern Gulf of Mexico
865 (Pigmy Basin). Quaternary Science Reviews 28, 3333–3347.
866 Montero-Serrano, J.C., Föllmi, K.B., Adatte, T., Spangenberg, J.E., Tribovillard, N., Fantasia, A., Suan,
867 G., 2015. Continental weathering and redox conditions during the early Toarcian Oceanic Anoxic
868 Event in the northwestern Tethys: Insight from the Posidonia Shale section in the Swiss Jura
869 Mountains. Palaeogeography, Palaeoclimatology, Palaeoecology 429, 83–99.
870 Montero-Serrano, J.C., Palarea-Albaladejo, J., Martin-Fernandez, J.A., Martinez-Santana, M., Gutierrez-
871 Martin, J.V., 2010b. Sedimentary chemofacies characterization by means of multivariate analysis.
872 Sedimentary Geology 228, 218–228. doi:10.1016/j.sedgeo.2010.04.013
873 Moore, T.S., Murray, R.W., Kurtz, A.C., Schrag, D.P., 2004. Anaerobic methane oxidation and the
874 formation of dolomite. Earth and Planetary Science Letters 229, 141–154.
875 doi:10.1016/j.epsl.2004.10.015
876 Mucci, A., Lansard, B., Miller, L.A., Papakyriakou, T.N., 2010. CO2 fluxes across the air-sea interface
877 in the southeastern Beaufort Sea: Ice-free period. Journal of Geophysical Research: Oceans 115,
878 n/a–n/a. doi:10.1029/2009JC005330

879 Naidu, A.S., Burrell, D.C., Wood, D.H., 1971. Clay Mineral Composition and Geologic Significance of
880 Some Beaufort Sea Sediments. Journal of Sedimentary Petrology 41, 691–694.
881 doi:10.1306/74D72329-2B21-11D7-8648000102C1865D
882 Naidu, A.S., Creager, J.S., Mowatt, T.C., 1982. Clay mineral dispersal patterns in the north Bering and
883 Chukchi Seas. Marine Geology 47, 1–15. doi:http://dx.doi.org/10.1016/0025-3227(82)90016-0
884 Naidu, A.S., Mowatt, T.C., 1983. Geological Society of America Bulletin Sources and dispersal patterns
885 of clay minerals in surface sediments from. doi:10.1130/0016-7606(1983)94<841
886 O'Brien, M.C., Macdonald, R.W., Melling, H., Iseki, K., 2006. Particle fluxes and geochemistry on the
887 Canadian Beaufort Shelf: Implications for sediment transport and deposition. Continental Shelf
888 Research 26, 41–81. doi:10.1016/j.csr.2005.09.007
889 Oksanen, J., Blanchet, F.G., Kindt, R., Legendre, P., Minchin, P.R., O'Hara, R.B., Simpson, G.L.,
890 Solymos, P., Stevens, M.H.H., Wagner, H., 2015. vegan: Community Ecology Package. R package
891 version 2.3-2.
892 Ortiz, J.D., Polyak, L., Grebmeier, J.M., Darby, D., Eberl, D.D., Naidu, S., Nof, D., 2009. Provenance of
893 Holocene sediment on the Chukchi-Alaskan margin based on combined diffuse spectral reflectance
894 and quantitative X-Ray Diffraction analysis. Global and Planetary Change 68, 73–84.
895 doi:10.1016/j.gloplacha.2009.03.020
896 Overland, J.E., Adams, J.M., Bond, N.A., 1999. Decadal variability of the Aleutian Low and its relation
897 to high-latitude circulation. Journal of Climate 12, 1542–1548.
898 Padgham, W.A., Fyson, W.K., 1992. The Slave Province: a distinct Archean craton. Canadian Journal of
899 Earth Sciences 29, 2072–2086. doi:10.1139/e92-165
900 Pancost, R.D., Bouloubassi, I., Aloisi, G., Damsté, J.S.S., the Medinaut Shipboard Scientific Party, 2001.
901 Three series of non-isoprenoidal dialkyl glycerol diethers in cold-seep carbonate crusts. Organic
902 Geochemistry 32, 695–707. doi:http://dx.doi.org/10.1016/S0146-6380(01)00015-8

903 Paull, C.K., Dallimore, S.R., Caress, D.W., Gwiazda, R., Melling, H., Riedel, M., Jin, Y.K., Hong, J.K.,
904 Kim, Y.-G., Graves, D., Sherman, A., Lundsten, E., Anderson, K., Lundsten, L., Villinger, H.,
905 Kopf, A., Johnson, S.B., Hughes Clarke, J., Blasco, S., Conway, K., Neelands, P., Thomas, H.,
906 Côté, M., 2015. Active mud volcanoes on the continental slope of the Canadian Beaufort Sea.
907 Geochemistry, Geophysics, Geosystems 16, 3160–3181. doi:10.1002/2015GC005928
908 Paull, C.K., Ussler, W., Dallimore, S.R., Blasco, S.M., Lorenson, T.D., Melling, H., Medioli, B.E.,
909 Nixon, F.M., McLaughlin, F.A., 2007. Origin of pingo-like features on the Beaufort Sea shelf and
910 their possible relationship to decomposing methane gas hydrates. Geophysical Research Letters 34,
911 n/a–n/a. doi:10.1029/2006GL027977
912
913 Pelletier, B. R., 1975. Sediment dispersal in the southern Beaufort Sea. Beaufort Sea Project. Technical
914 Report No. 25a, Department of the Environment, Victoria, British Columbia, 80 pp.
915 Pickart, R.S., 2004. Shelfbreak circulation in the Alaskan Beaufort Sea: Mean structure and variability.
916 Journal of Geophysical Research: Oceans 109, n/a–n/a. doi:10.1029/2003JC001912
917 Reimann, C., Filzmoser, P., Garrett, R., Dutter, R., 2008. Statistical data analysis explained: applied
918 environmental statistics with R. John Wiley & Sons.
919 Reimnitz, E., Clayton, J.R., Kempema, E.W., Payne, J.R., Weber, W.S., 1993. Interaction of rising frazil
920 with suspended particles: tank experiments with applications to nature. Cold Regions Science and
921 Technology 21, 117–135. doi:http://dx.doi.org/10.1016/0165-232X(93)90002-P
922 Richerol, T., Rochon, A., Blasco, S., Scott, D.B., Schell, T.M., Bennett, R.J., 2008a. Evolution of paleo
923 sea-surface conditions over the last 600 years in the Mackenzie Trough, Beaufort Sea (Canada).
924 Marine Micropaleontology 68, 6–20. doi:10.1016/j.marmicro.2008.03.003
925 Richerol, T., Rochon, A., Blasco, S., Scott, D.B., Schell, T.M., Bennett, R.J., 2008b. Distribution of
926 dinoflagellate cysts in surface sediments of the Mackenzie Shelf and Amundsen Gulf, Beaufort Sea

927 (Canada). Journal of Marine Systems 74, 825–839. doi:10.1016/j.jmarsys.2007.11.003
928 Saint-Ange, F., Kuus, P., Blasco, S., Piper, D.J.W., Clarke, J.H., MacKillop, K., 2014. Multiple failure
929 styles related to shallow gas and fluid venting, upper slope Canadian Beaufort Sea, northern
930 Canada. Marine Geology 355, 136–149. doi:10.1016/j.margeo.2014.05.014
931 Schell, T.M., Moss, T.J., Scott, D.B., Rochon, A., 2008. Paleo-sea ice conditions of the Amundsen Gulf,
932 Canadian Arctic Archipelago: Implications from the foraminiferal record of the last 200 years.
933 Journal of Geophysical Research: Oceans 113, 1–14. doi:10.1029/2007JC004202
934 Schoster, F., Behrends, M., Muller, R., Stein, R., Washner, M., 2000. Modern river discharge and
935 pathways of supplied material in the Eurasian Arctic Ocean: Evidence from mineral
936 assemblagesand major and minor element distribution. International Journal of Earth Sciences 89,
937 486–495. doi:10.1007/s005310000120
938 Scott, D.B., Schell, T., Rochon, A., Blasco, S., 2008. Benthic foraminifera in the surface sediments of
939 the Beaufort Shelf and slope, Beaufort Sea, Canada: Applications and implications for past sea-ice
940 conditions. Journal of Marine Systems 74, 840–863. doi:10.1016/j.jmarsys.2008.01.008
941 Scott, D.B., Schell, T., St-Onge, G., Rochon, A., Blasco, S., 2009. Foraminiferal assemblage changes
942 over the last 15,000 years on the Mackenzie-Beaufort Sea Slope and Amundsen Gulf, Canada:
943 Implications for past sea ice conditions. Paleoceanography 24, 1–20. doi:10.1029/2007PA001575
944 Shearer, J.M., Macnab, R.F., Pelletier, B.R., Smith, T.B., 1971. Submarine Pingos in the Beaufort Sea.
945 Science 174, 816–818.
946 Simon, Q., St-Onge, G., Hillaire-Marcel, C., 2012. Late Quaternary chronostratigraphic framework of
947 deep Baffin Bay glaciomarine sediments from high-resolution paleomagnetic data. Geochemistry,
948 Geophysics, Geosystems 13, 1–24. doi:10.1029/2012GC004272
949 Stein, R., 2008. Arctic Ocean Sediments: Processes, Proxies, and Paleoenvironment, Developments in
950 Marine Geology, Developments in Marine Geology. Elsevier. doi:10.1016/S1572-5480(08)00002-

951 X
952 Stokes, C.R., Clark, C.D., Winsborrow, C.M., 2006. Subglacial bedform evidence for a major palaeo-ice
953 stream and its retreat phases in Amundsen Gulf, Canadian Arctic Archipelago. Journal of
954 Quaternary Science 21, 399–412. doi:10.1002/jqs.991
955 Stoner, J.S., St-Onge, G., 2007. Chapter Three Magnetic Stratigraphy in Paleoceanography: Reversals,
956 Excursions, Paleointensity, and Secular Variation. Developments in Marine Geology 1, 99–138.
957 doi:10.1016/S1572-5480(07)01008-1
958 Tremblay, J.-É., Raimbault, P., Garcia, N., Lansard, B., Babin, M., Gagnon, J., 2014. Impact of river
959 discharge, upwelling and vertical mixing on the nutrient loading and productivity of the Canadian
960 Beaufort Shelf. Biogeosciences 11, 4853–4868. doi:10.5194/bg-11-4853-2014
961 Tribovillard, N., Algeo, T.J., Lyons, T., Riboulleau, A., 2006. Trace metals as paleoredox and
962 paleoproductivity proxies: an update. Chemical geology 232, 12–32.
963 van den Boogaart, K.G., Tolosana-Delgado, R., 2008. “compositions”: A unified R package to analyze
964 compositional data. Computers and Geosciences 34, 320–338. doi:10.1016/j.cageo.2006.11.017
965 Viscosi-Shirley, C., Mammone, K., Pisias, N., Dymond, J., 2003. Clay mineralogy and multi-element
966 chemistry of surface sediments on the Siberian-Arctic shelf: Implications for sediment provenance
967 and grain size sorting. Continental Shelf Research 23, 1175–1200. doi:10.1016/S0278-
968 4343(03)00091-8
969 Vogt, C., 1997. Regional and temporal variations of mineral assemblages in Arctic Ocean sediments as
970 climatic indicator during glacial/interglacial changes. Reports on Polar Research 251, 309.
971 von Eynatten, H., Barcelo-Vidal, C., Pawlowsky-Glahn, V., 2003. Composition and Discrimination of
972 Sandstones: A Statistical Evaluation of Different Analytical Methods. Journal of Sedimentary
973 Research 73, 47–57. doi:10.1306/070102730047
974 von Eynatten, H., Tolosana-Delgado, R., Karius, V., Bachmann, K., Caracciolo, L., 2016. Sediment

975 generation in humid Mediterranean setting: Grain-size and source-rock control on sediment
976 geochemistry and mineralogy (Sila Massif, Calabria). Sedimentary Geology 336, 68–80.
977 doi:http://dx.doi.org/10.1016/j.sedgeo.2015.10.008
978 Vonk, J.E., Giosan, L., Blusztajn, J., Montlucon, D., Pannatier, E.G., McIntyre, C., Wacker, L.,
979 Macdonald, R.W., Yunker, M.B., Eglinton, T.I., 2015. Spatial variations in geochemical
980 characteristics of the modern Mackenzie Delta sedimentary system. Geochimica et Cosmochimica
981 Acta 171, 100–120. doi:http://dx.doi.org/10.1016/j.gca.2015.08.005
982 Wagner, A., Lohmann, G., Prange, M., 2011. Arctic river discharge trends since 7ka BP. Global and
983 Planetary Change 79, 48–60. doi:10.1016/j.gloplacha.2011.07.006
984 Weltje, G.J., 1997. End-member modeling of compositional data: Numerical-statistical algorithms for
985 solving the explicit mixing problem. Mathematical Geology 29, 503–549. doi:10.1007/BF02775085
986 White, A.F., Bullen, T.D., Schulz, M.S., Blum, A.E., Huntington, T.G., Peters, N.E., 2001. Differential
987 rates of feldspar weathering in granitic regoliths. Geochimica et Cosmochimica Acta 65, 847–869.
988 doi:http://dx.doi.org/10.1016/S0016-7037(00)00577-9
989 Yang, L.U., Xiaoming, S.U.N., Zhiyong, L.I.N., Hongfeng, L.U., 2014. Authigenic Carbonate
990 Mineralogy , South China Sea and Its Relationship with Cold Seep Activity 88.
991 Young, R.A., 1993. The Rietveld Method. International Union of Crystallography Monographs on
992 Crystallography 5. [Chester, England]: Oxford; New York: International Union of Crystallograhy;
993 Oxford University Press, 308 p.
994
995 **Figure captions**
996
997 **Figure 1**. Map of the Beaufort Sea and Amundsen Gulf illustrating the location of surface sediment
998 samples used in this study. Partially infilled cross-shelf channels (IT: Ikit Trough, KC: Kugmallit

Channel, NC: Niglik Channel) and distribution of mud volcanoes across the Beaufort Shelf are also illustrated (Blasco et al., 2013). MT represents the Mackenzie Trough; the thick white arrows represent the coastal surface circulation which is dominated by the Beaufort Undercurrent (here represented under westerly influence); the black line indicates the maximum extent of the Mackenzie River Plume; the light blue shading represents the extent of the spring ice-free zone.

Figure 2. Mean grain-size (A) and sorting (B) distributions (phi units) for the Mackenzie-Beaufort Sea Slope and Amundsen Gulf sediments. Note that in (B) all sediment samples are poorly sorted, however, relatively higher sorting (values up to 1.75) is found in some samples from the mud volcanoes area, in the Canadian Beaufort Shelf as well as in the southwestern Banks Island.

Figure 3. End-member modelling analyses (EMMA) performed on the grain-size distribution of the detrital fraction from the Canadian Beaufort Shelf and Amundsen Gulf. (A) The grain-size distribution of the first three end-members accounts for more than 91% of the total variance. (B) Three representative unmixed grain-size distributions derived from EMMA. (C) Log(EM1/EM2+EM3) and (D) Log(EM2/EM3) end-member ratios, which represent the relative proportion between clay/silts and medium-silt/coarse-silt, respectively.

Figure 4. (A) Hysteresis loop curves for three representative samples from the Mackenzie Trough-Canadian Beaufort Shelf (MT-CBS), central Amundsen Gulf (cAG), and southwestern Banks Island (SWBI); and (B) Mrs/Ms and Hcr/Hc crossplot (Day plot) illustrating the magnetic grain size SD (single domain), PSD (pseudo-single domain), and MD (multi-domain) zonation (adapted from Day, 1977).

Figure 5. Magnetic properties of surface sediments from the Canadian Beaufort Shelf and Amundsen Gulf. (A) Spatial distribution of magnetic susceptibility (k_{lf}); (B) Spatial distribution of Mrs/Ms ratio; (C) Spatial distribution of Hcr/Hc ratio. Note that all magnetic parameters show similar spatial distributions.

Figure 6. (A) Biplot of the PC-1 versus PC-2 obtained from the log-centred transformation of the bulk mineralogical data from the Canadian Beaufort Shelf and Amundsen Gulf sediments. (B) Loadings derived from the principal component analysis illustrating the weight (>0.1) of each mineral in the definition of each PC score.

Figure 7. Map of PC-1 and PC-2 scores derived from the bulk mineralogical data from the Canadian Beaufort Shelf and Amundsen Gulf sediments.

Figure 8. (A) Al_2O_3-SiO_2-CaO ternary plot shows the overall composition of surface sediments from the Canadian Beaufort Shelf and Amundsen Gulf in comparison with average shale (adapted from Brumsack, 1989). (B) Log(Fe/Al) versus Log(Mn/Al).

Figure 9. Box plots of the enrichment factors (EF) of redox-sensitive elements (Mn, Fe, V, Cr, Zn) from the Mackenzie Trough-Canadian Beaufort Shelf (MT-CBS), central Amundsen Gulf (cAG), and southwestern Banks Island (SWBI) sediments.

Figure 10. (A) Biplot of the PC-1 versus PC-2 obtained from the log-centred transformation of the major-, minor-, and trace-element data from the Canadian Beaufort Shelf and Amundsen Gulf sediments.

(B) Loadings derived from the principal component analysis illustrating the weight (>0.1) of each element in the definition of each PC score.

Figure 11. (A) Spatial distribution of Log(Mn/Al). (B-C) Map of PC-1 and PC-2 scores derived from the major-, minor-, and trace-element data from the Canadian Beaufort Shelf and Amundsen Gulf sediments.

Figure 12. Relationship between siliciclastic mean grain size (phi units), bulk mineralogy (PC-1 score), elemental geochemistry (PC-1 score), magnetic susceptibility [Log(k_{lf})], and Log(Hcr/Hc).

Figure 13. Silhouette (A) and principal coordinate ordination (B) plots resulting from the fuzzy c-means clustering analysis based on the bulk mineralogical data from the Canadian Beaufort Shelf and Amundsen Gulf sediments. The parameters listed on the right-hand side in (A) represent of number of sample in each cluster and their membership's values. 100% of the cluster memberships are correctly classified. In (B) each cluster is associated with a small "star" whose segment radiuses are proportional to its membership coefficient.

Figure 14. Generalized map summarizing the main sedimentary provinces defined in this study. The thick white arrows represent surface currents.

Figure 15. K-feldspar/plagioclase versus quartz/(K-feldspar+plagioclase) diagram illustrating the mineralogical difference between some circum-Arctic regions. Surface marine sediments from the Canadian Beaufort Sea (this study), Amundsen Gulf (this study), Eurasian shelf (Stein, 2008; Bazhenova, 2012), Bering Strait (Linsen et al., 2014), as well as continental sediments from the northern Yukon Territory, Tuktoyaktuk Peninsula, Cape Bathurst, and Banks Island (Vogt, 1997) are plotted.

Supplementary tables

Table S1. Frequency-dependent susceptibilities data for the some bulk sediments samples from the Mackenzie Trough-Canadian Beaufort Shelf (MT-CBS), central Amundsen Gulf (cAG), southwestern Banks Island (SWBI;), and mud volcanoes (MV) sediments.

Supplementary figures

Figure S1. Box plots of the main bulk mineral components present in the different sedimentary regions (Mackenzie Trough-Canadian Beaufort Shelf, mud volcanoes, central Amundsen Gulf, and southwestern Banks Island). The box plots show the median (horizontal line) and the box includes 50% of the distribution. Small crosses represent outliers.

Figure S2. Box plots of the major-, minor-, and trace-element concentrations for the different sedimentary regions (Mackenzie Trough-Canadian Beaufort Shelf, mud volcanoes, central Amundsen Gulf, and southwestern Banks Island). The box plots show the median (horizontal line) and the box includes 50% of the distribution. Small crosses represent outliers.

Figure S3. Photography (A) and scanning electron microscopic (B) images of white crusts observed in a representative mud volcano sediment sample (2004-804-609). EDS (Energy-dispersive X-ray spectroscopy) spectrum of white crusts (C). The red circle indicates the location of the EDS analysis. EDS spectrum is consistent with the presence of Ca-Mg authigenic carbonates (notably, low Mg-calcite). Na and Cl peaks reflect the high salt content of the pore waters. Other peaks (e.g., Si, Al, Fe, and P) are

interpreted as background detrital sediment signals. Sulfides (such as, pyrite and greigite) were not observed in the SEM-EDS analysis. X-ray diffractogram (D) of the bulk sediment sample showing the presence of dolomite, calcite and low Mg-calcite. The salt content is represented by the halite peak. Note that the bulk sediment samples were not rinsed with distilled water for the SEM-EDS analysis, hence the presence of salt.

Figure 1.

Figure 1

(Doubled column-full page width)

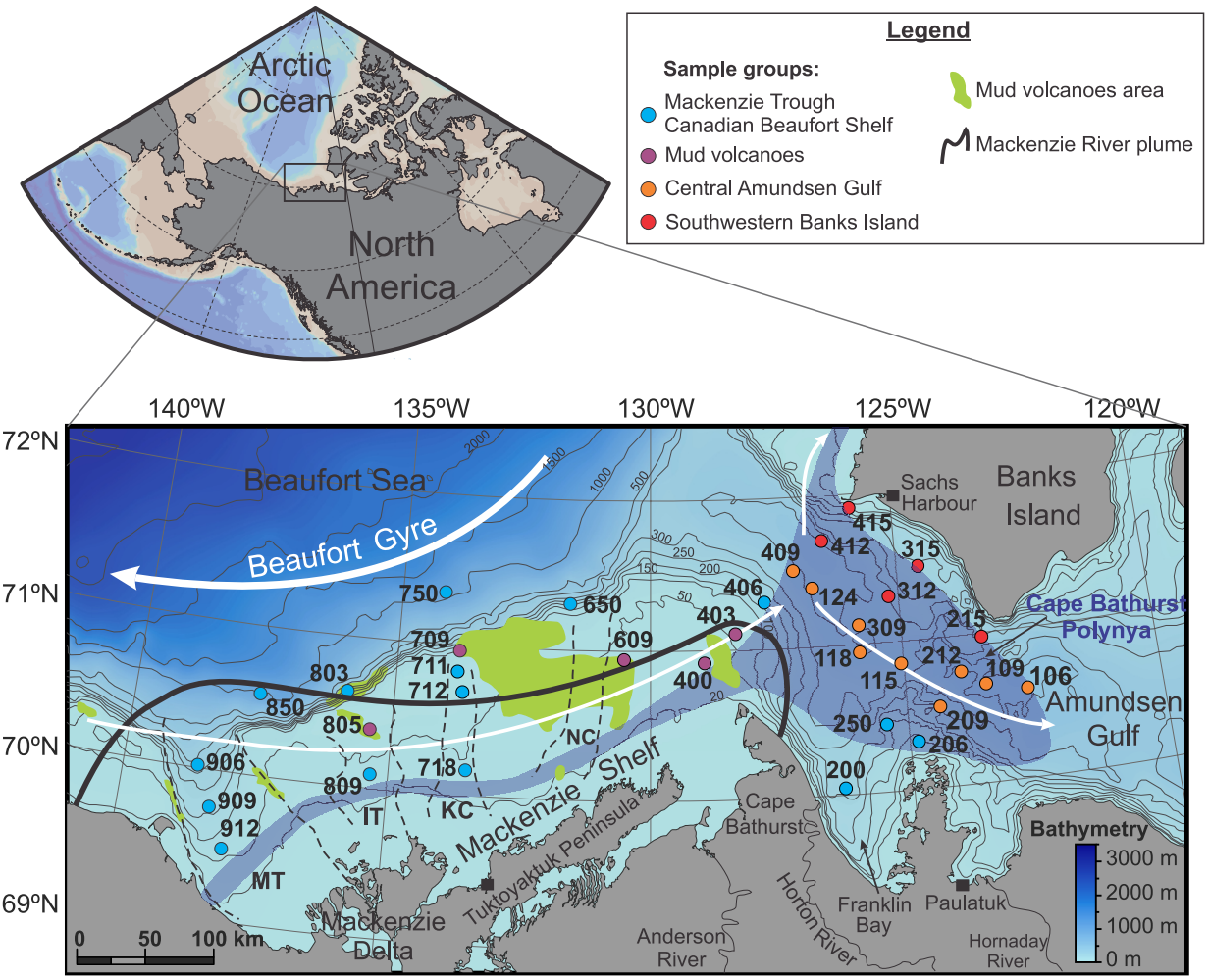

Figure 2.

Figure 2

(Double column - full page width)

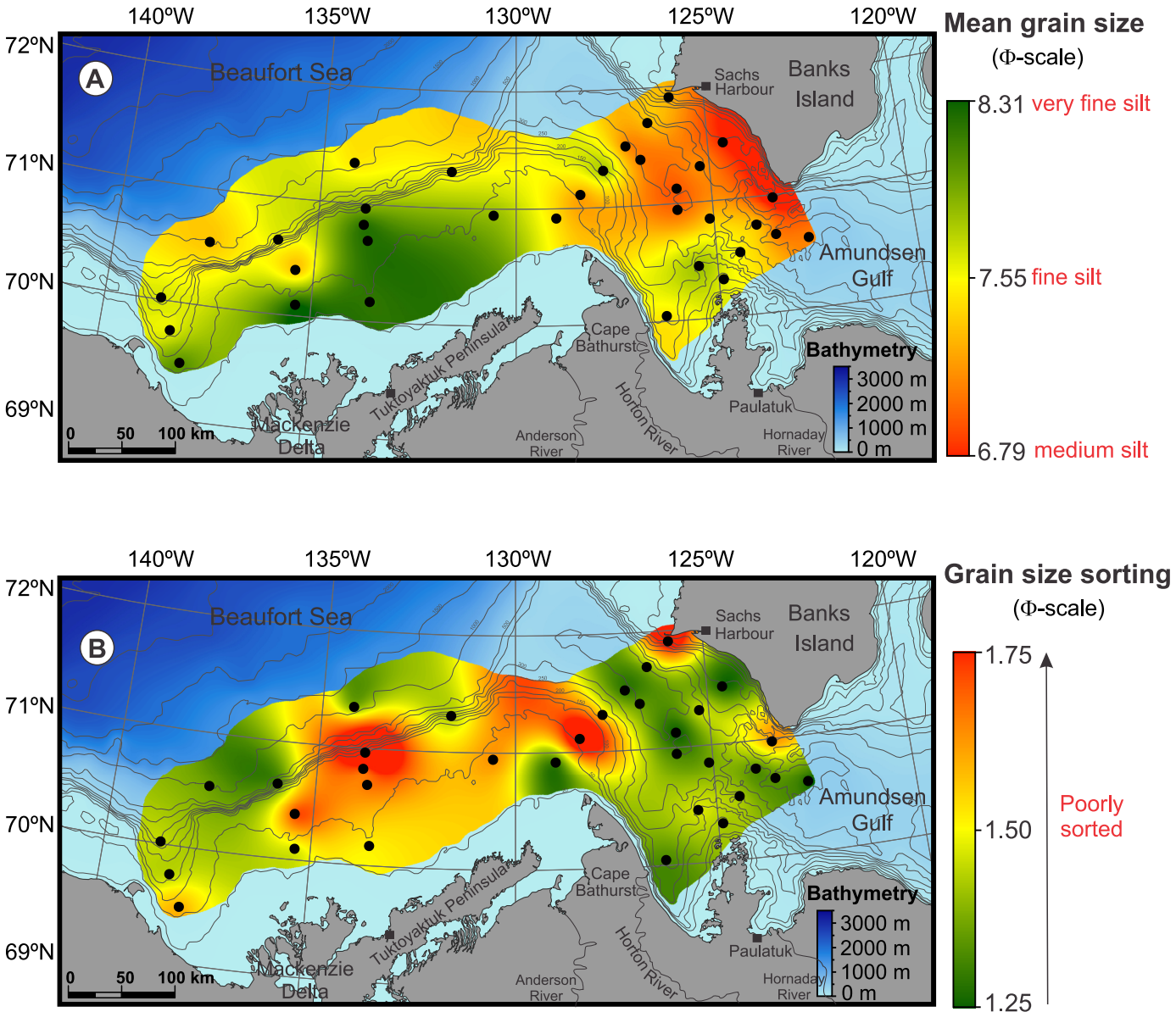

Figure 3.

Figure 3

(Double column - full page width)

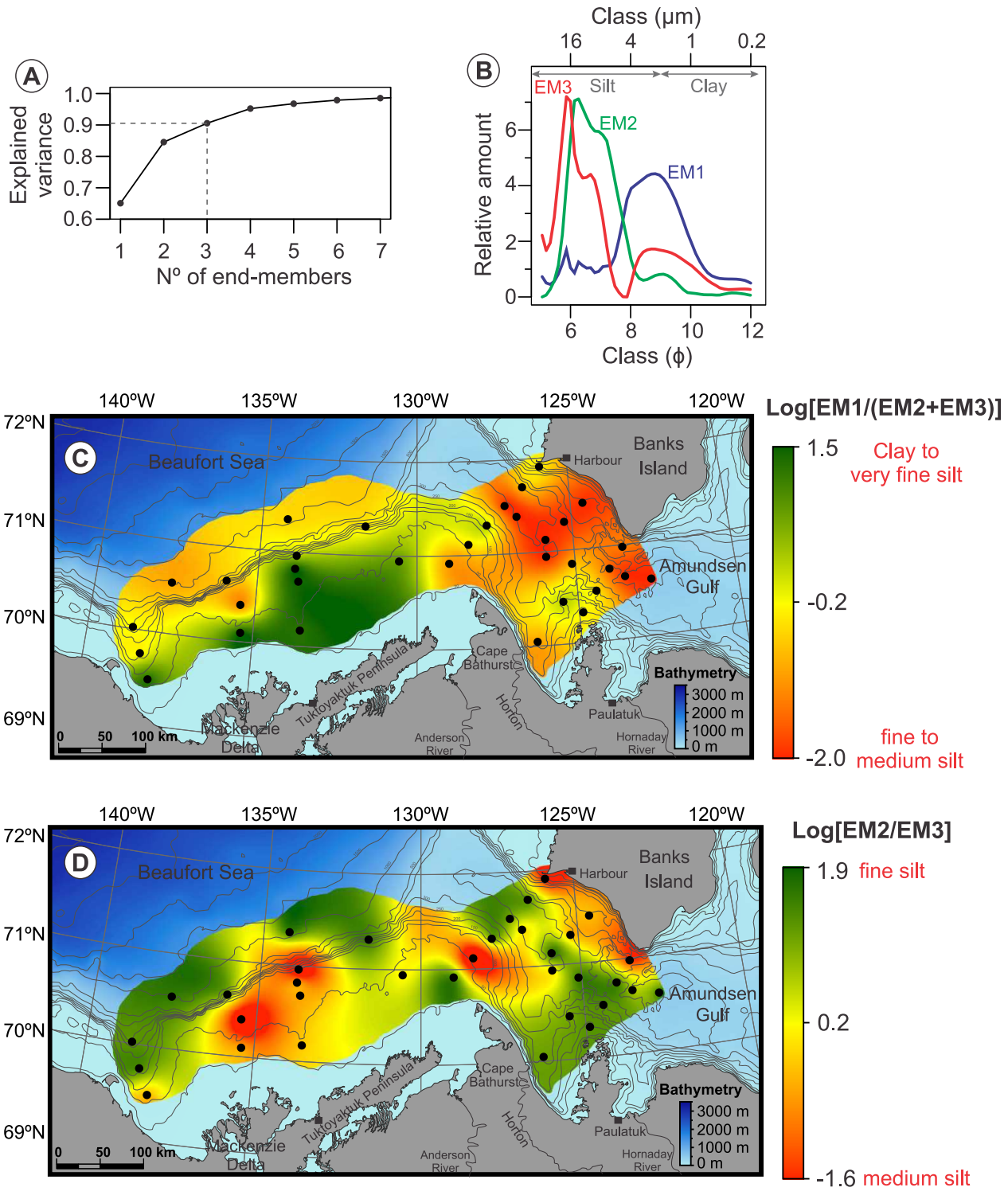

Figure 4.

Figure 4

(1.5 column)

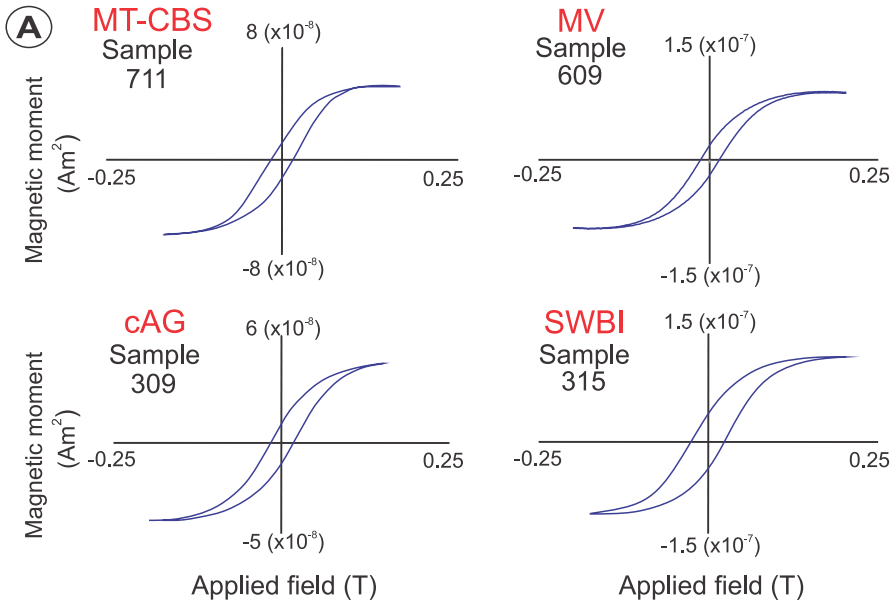

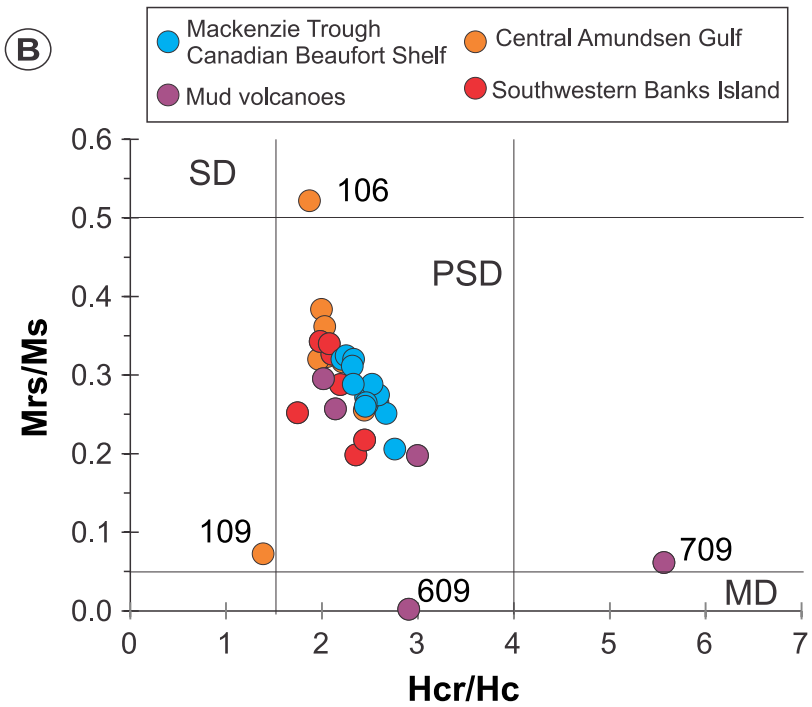

Figure 5.

Figure 5

(Double column - full page width)

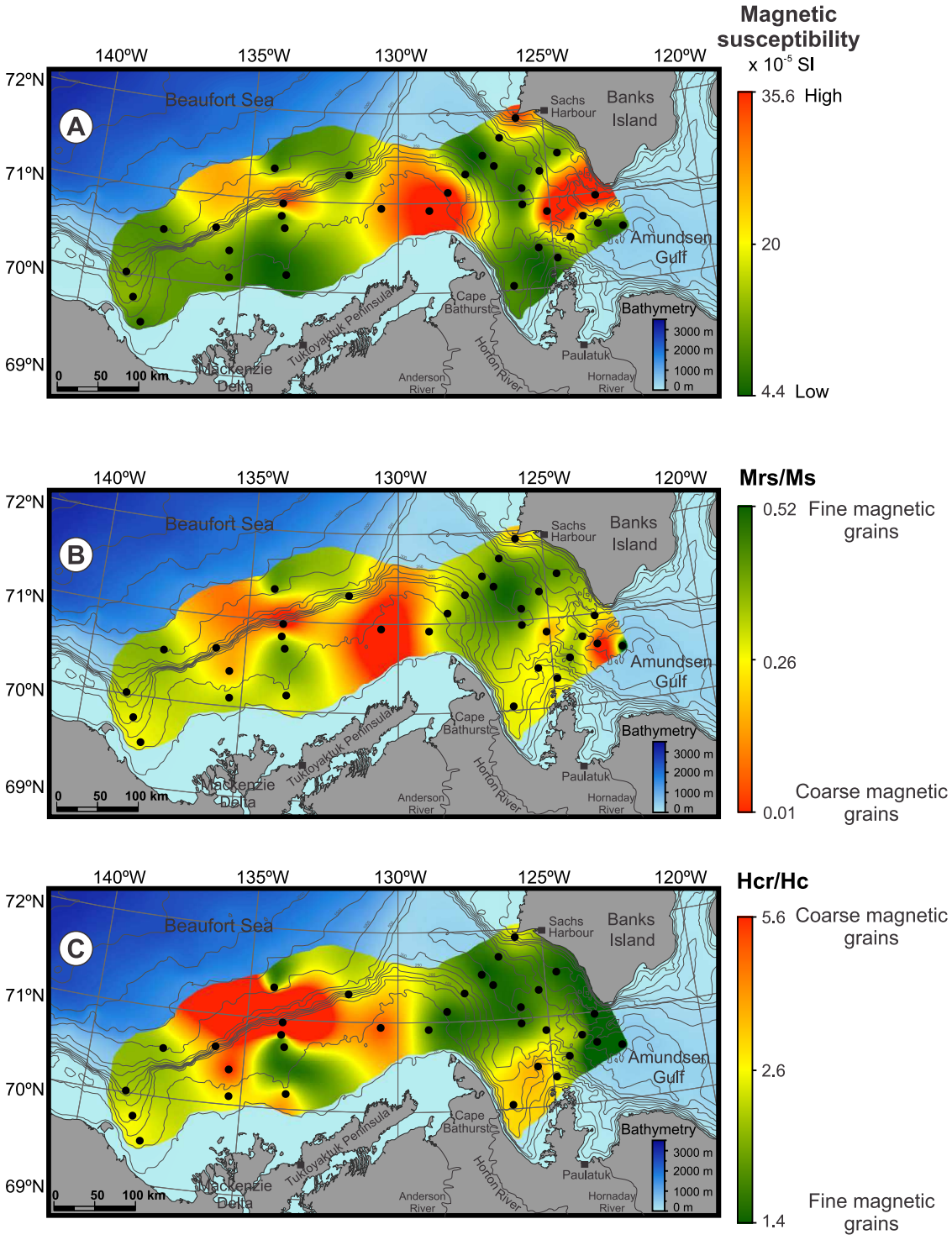

Figure 6.

Figure 6

(Double column - full page width)

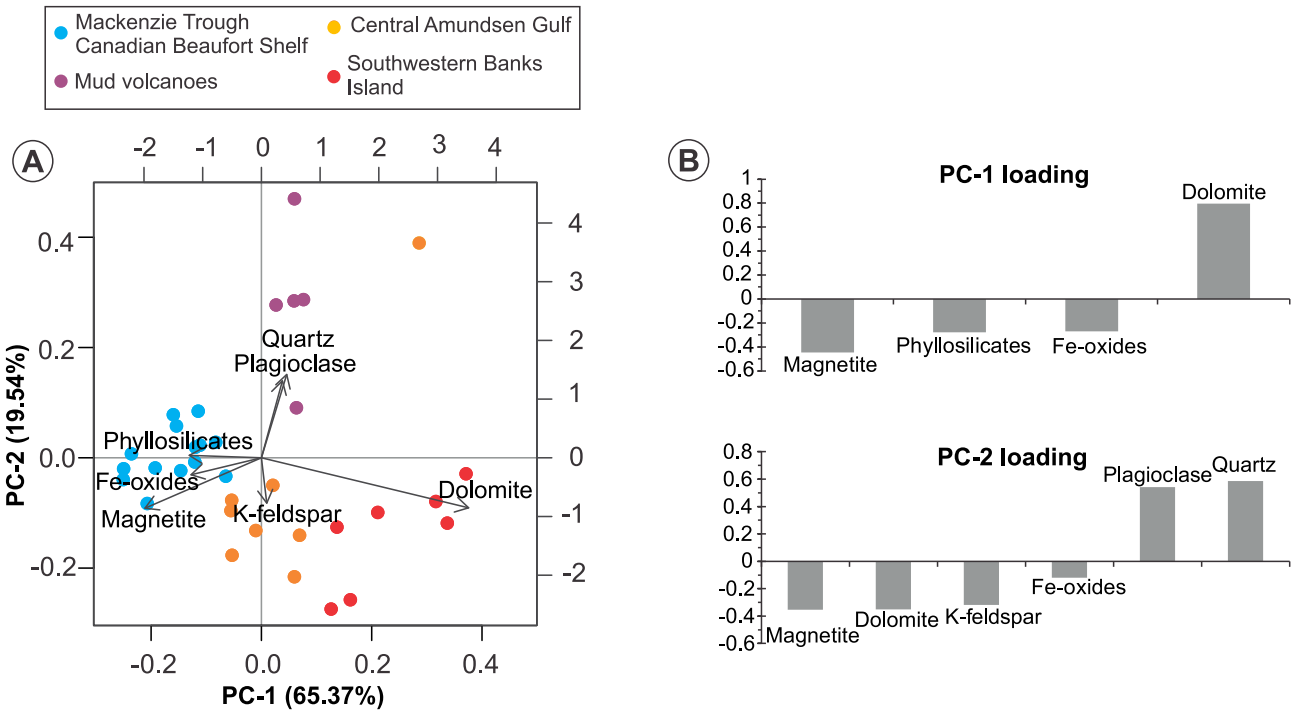

Figure 7.

Figure 7

(Double column - full page width)

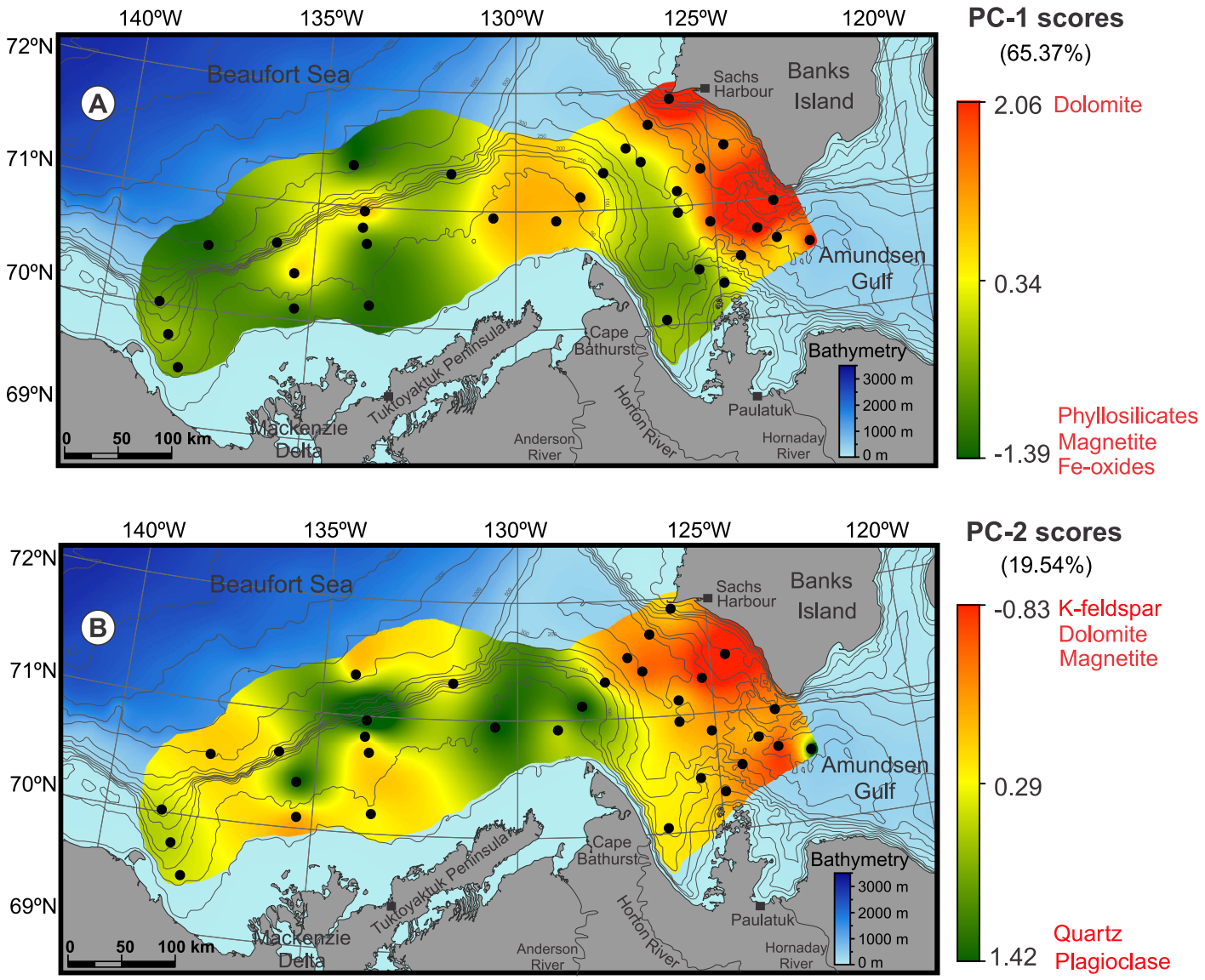

Figure 8.

Figure 8

(Double column - full page width)

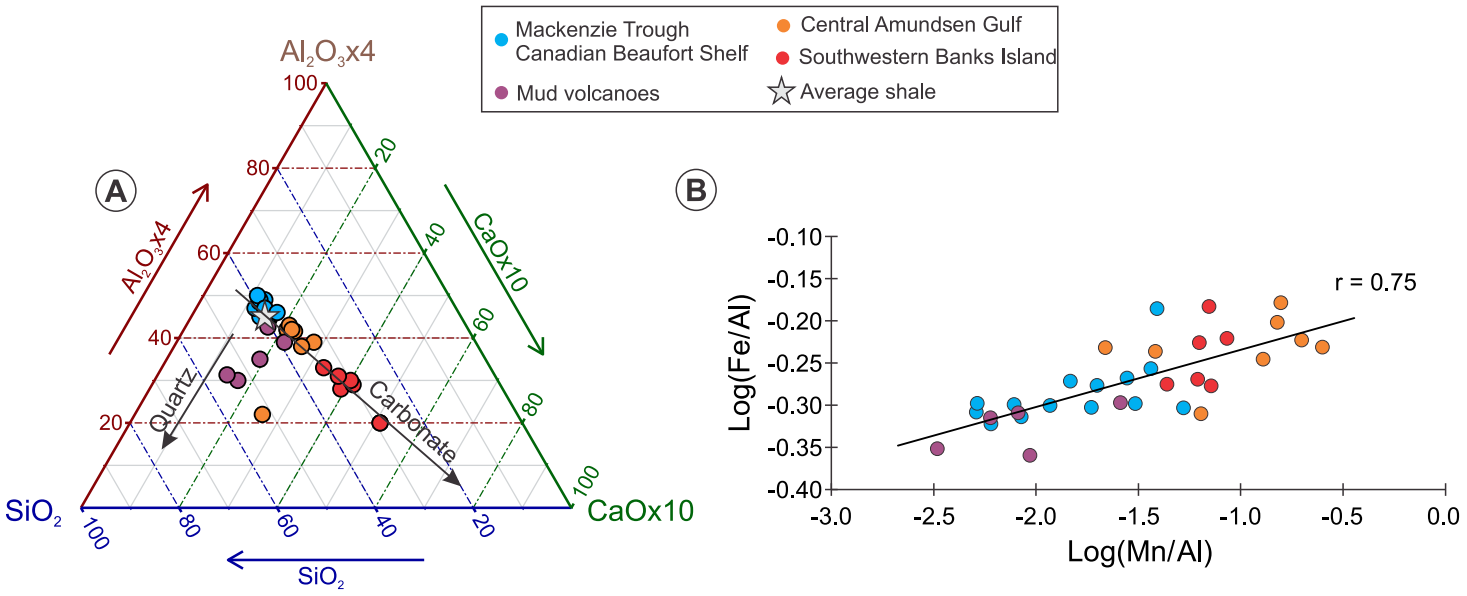

Figure 9.

Figure 9

(Double column - full page width)

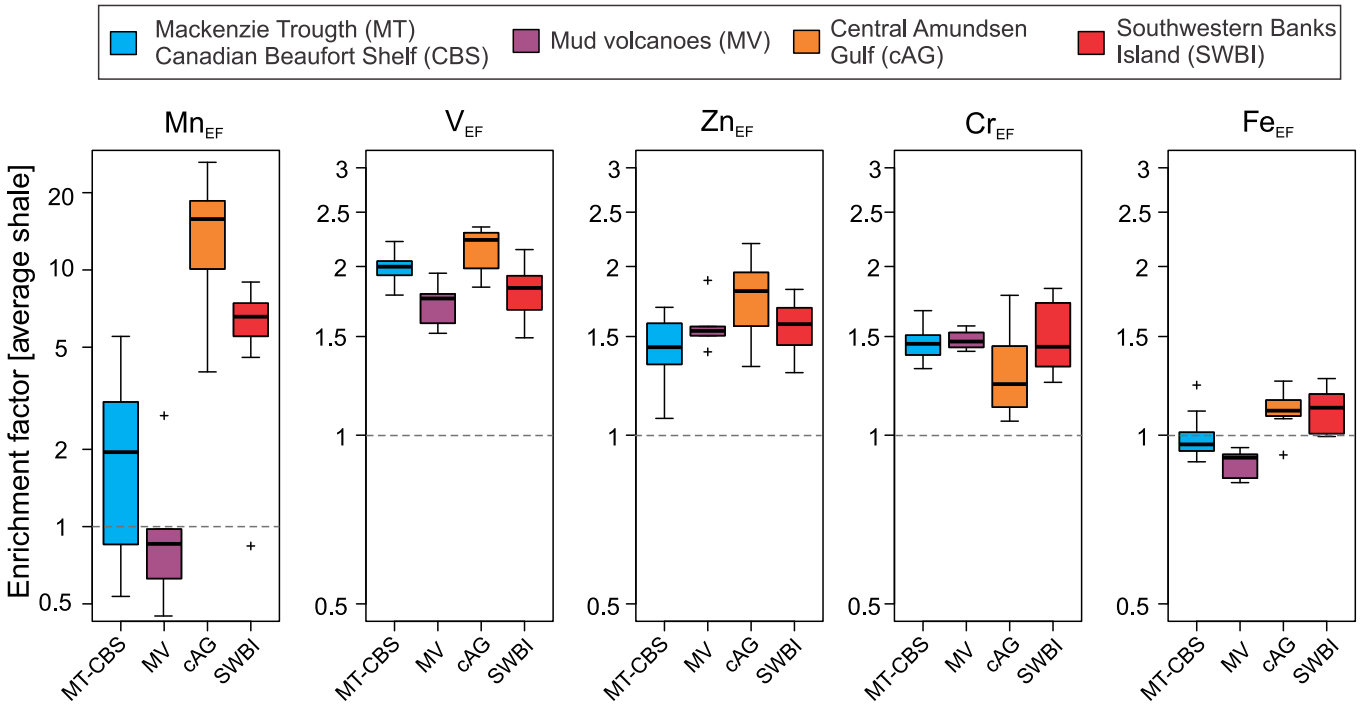

Figure 10.

Figure 10

(Double column - full page width)

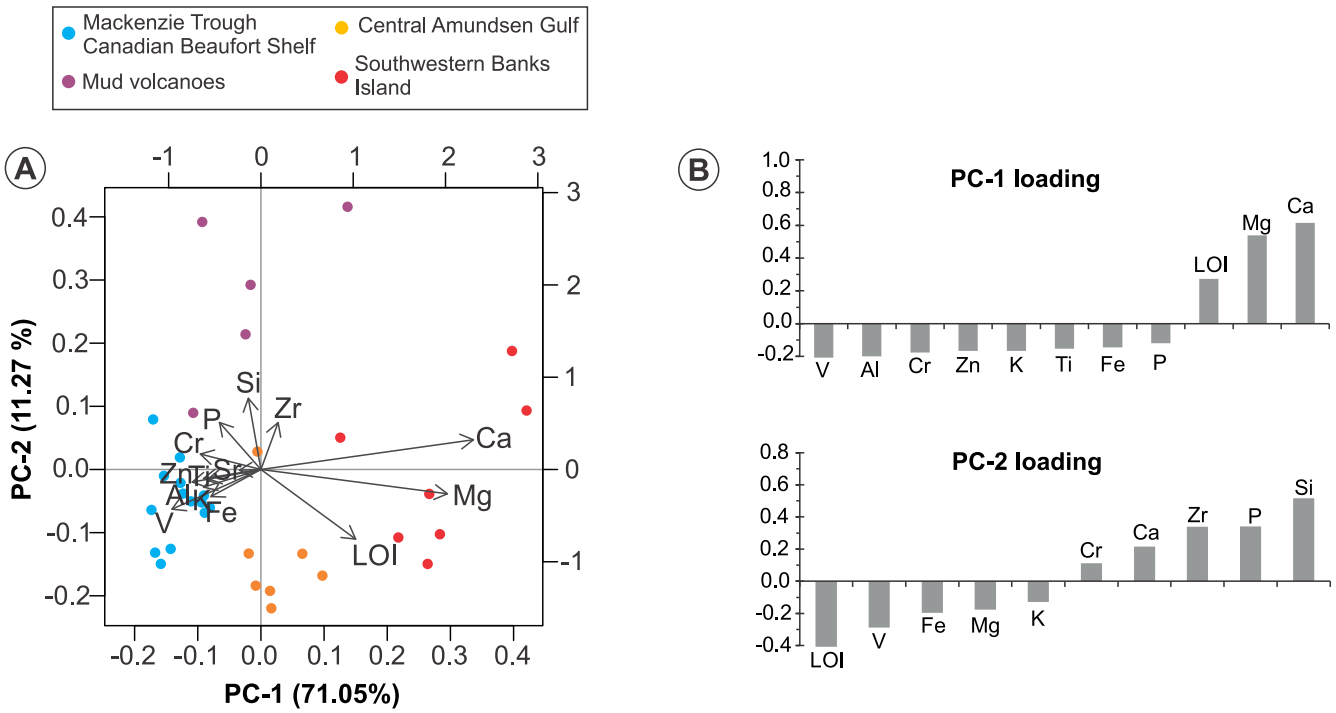

Figure 11.

Figure 11

(Double column - full page width)

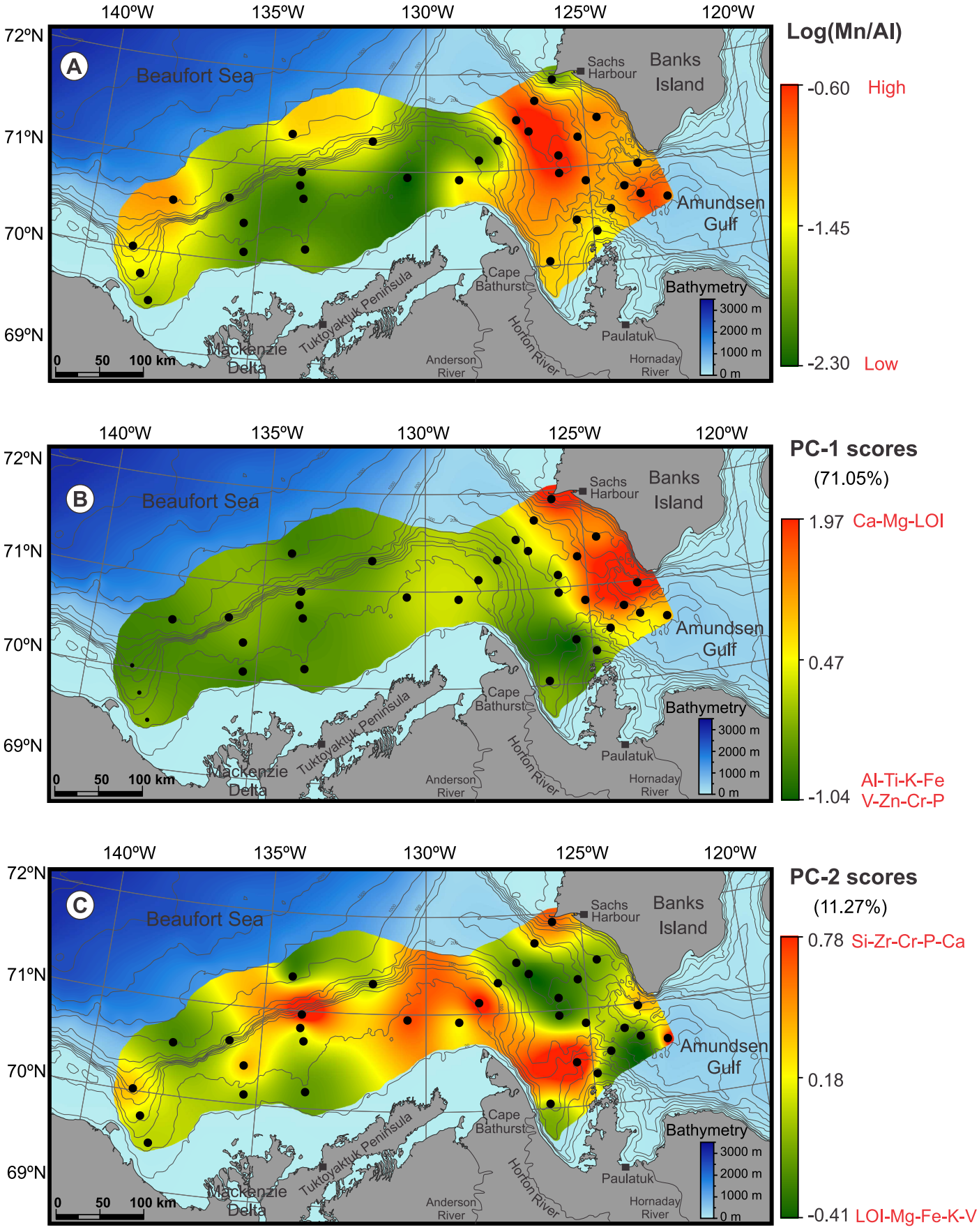

Figure 12.

Figure 12

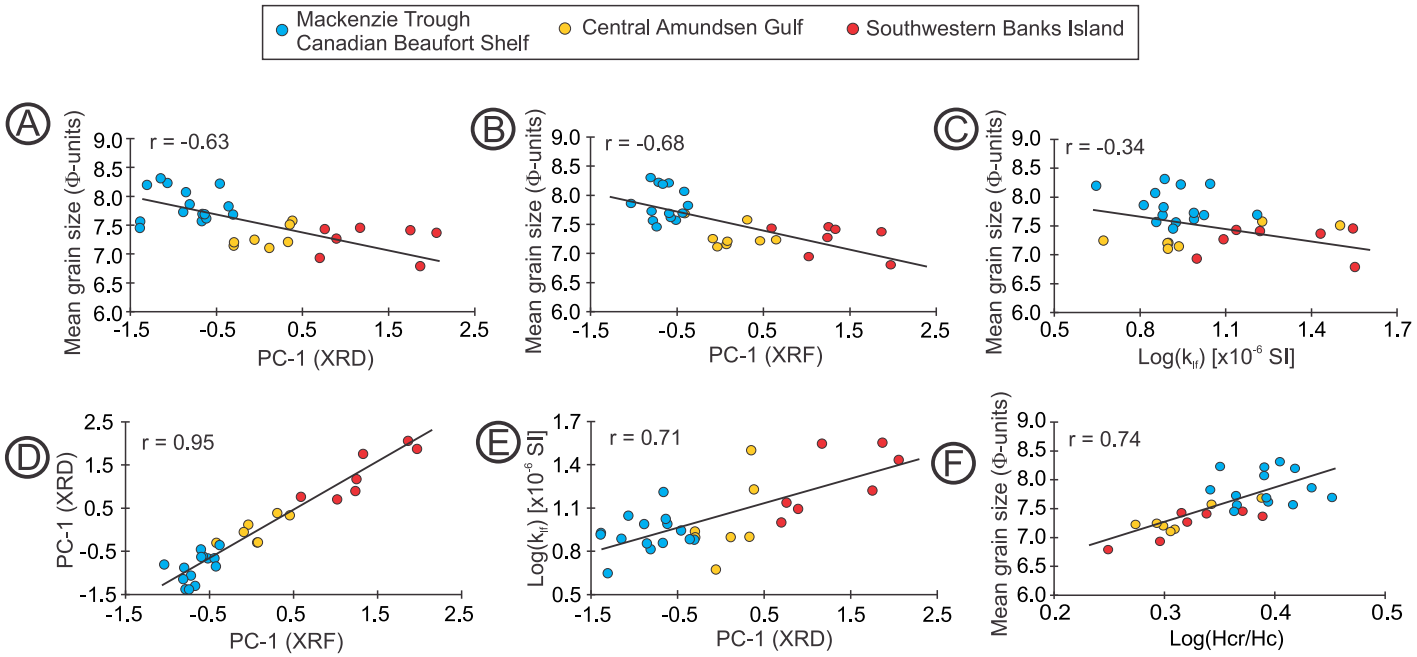
Mackenzie Trough
Canadian Beaufort Shelf
Central Amundsen Gulf
Southwestern Banks Island
A
r = -0.63
Mean grain size (Φ-units)
PC-1 (XRD)
B
r = -0.68
Mean grain size (Φ-units)
PC-1 (XRF)
C
r = -0.34
Mean grain size (Φ-units)
Log(k_lf) [x10^-6 SI]
D
r = 0.95
PC-1 (XRD)
PC-1 (XRF)
E
r = 0.71
Log(k_lf) [x10^-6 SI]
PC-1 (XRD)
F
r = 0.74
Mean grain size (Φ-units)
Log(Hcr/Hc)

Figure 13.

Figure 13

(Double column - full page width)

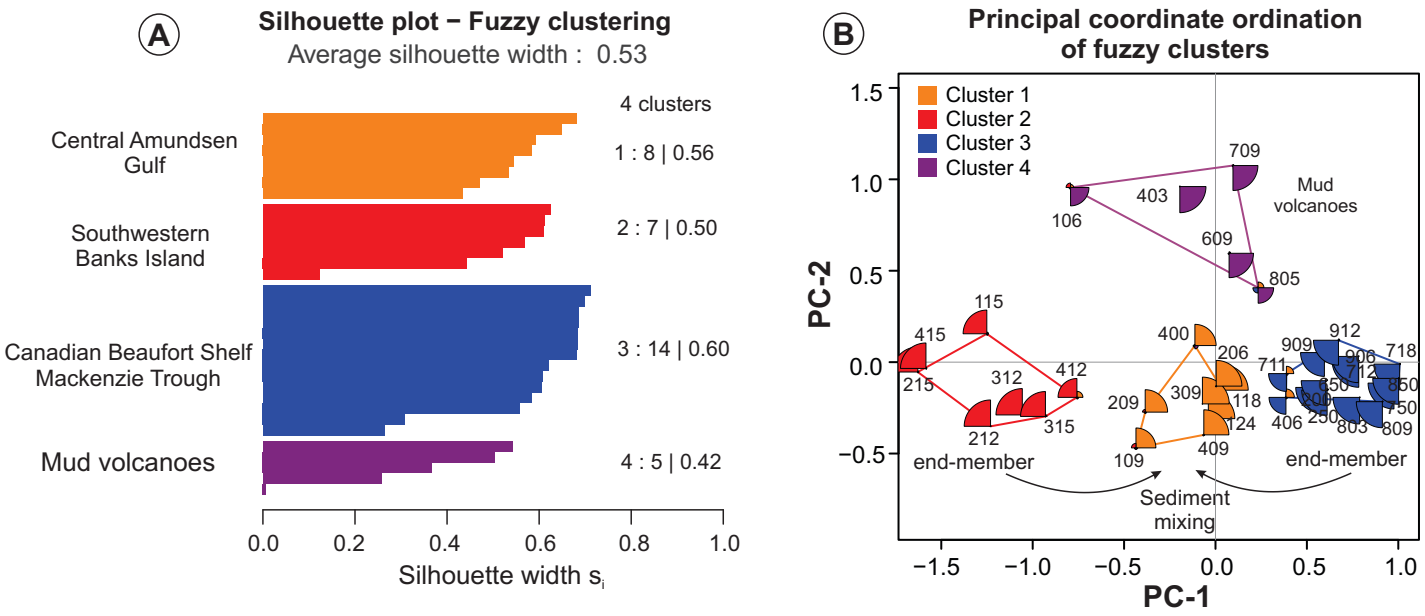

Figure 14.

Figure 14

(Double column - full page width)

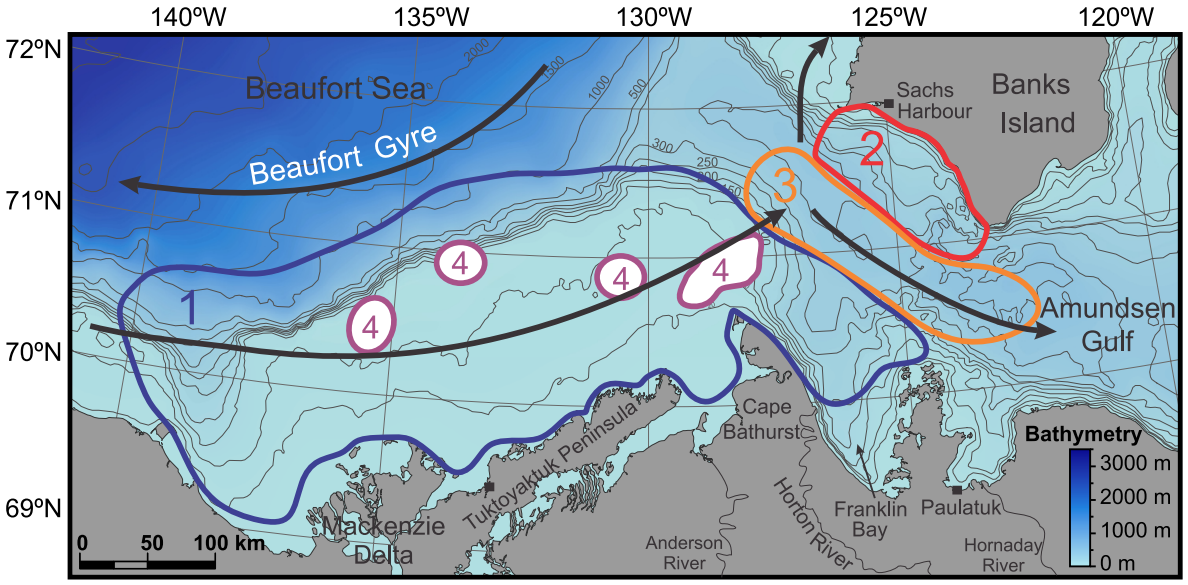

Sedimentary provinces:

1. Preferential influence of discharge of the Mackenzie River
   high phyllosilicates, Fe oxides, magnetite and Al-K-Ti-Fe-Cr-V-Zn-P contents
2. Preferential influence of coastal erosion
   high dolomite, K-feldspar and Ca-Mg-LOI contents
3. Transition zone (mixture characteristics from zones 1 and 2)
   intermediate phyllosilicates, magnetite, K-feldspar, dolomite, and Al-K-Ti-Fe-Mn-V-Zn-Sr-Ca-Mg-LOI contents
4. Zone influenced by mud volcanoes
   high quartz-plagioclase-authigenic carbonates and Si-Zr contents, high magnetic susceptibility

Figure 15.

Figure 15

(Double column - full page width)

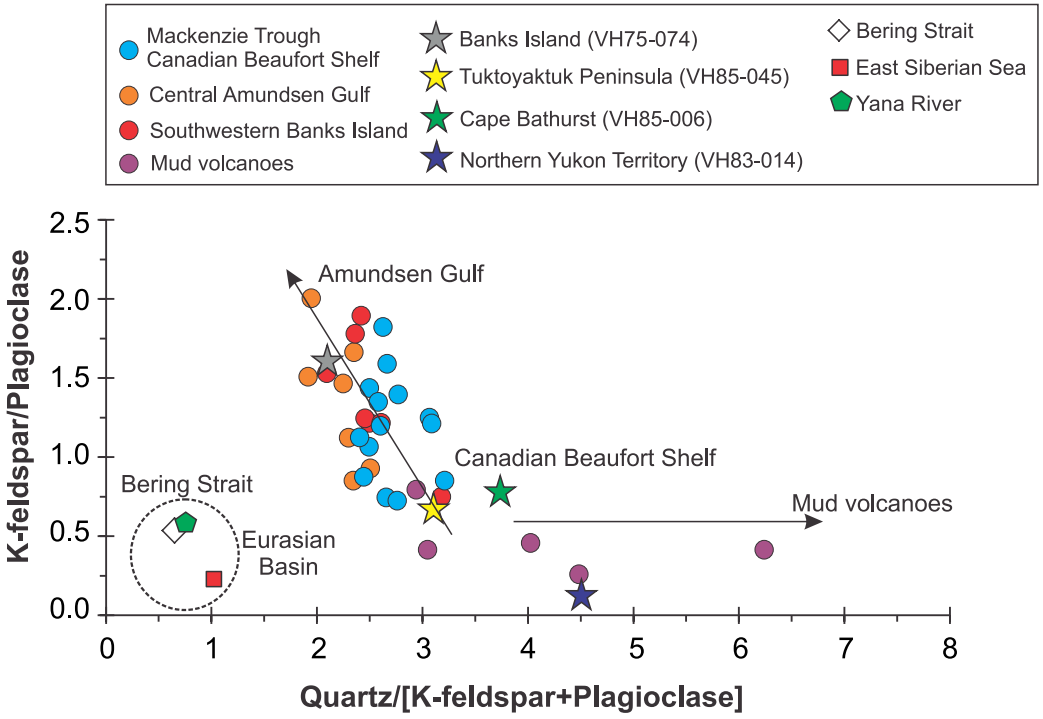

Graphical abstract.

Graphical abstract

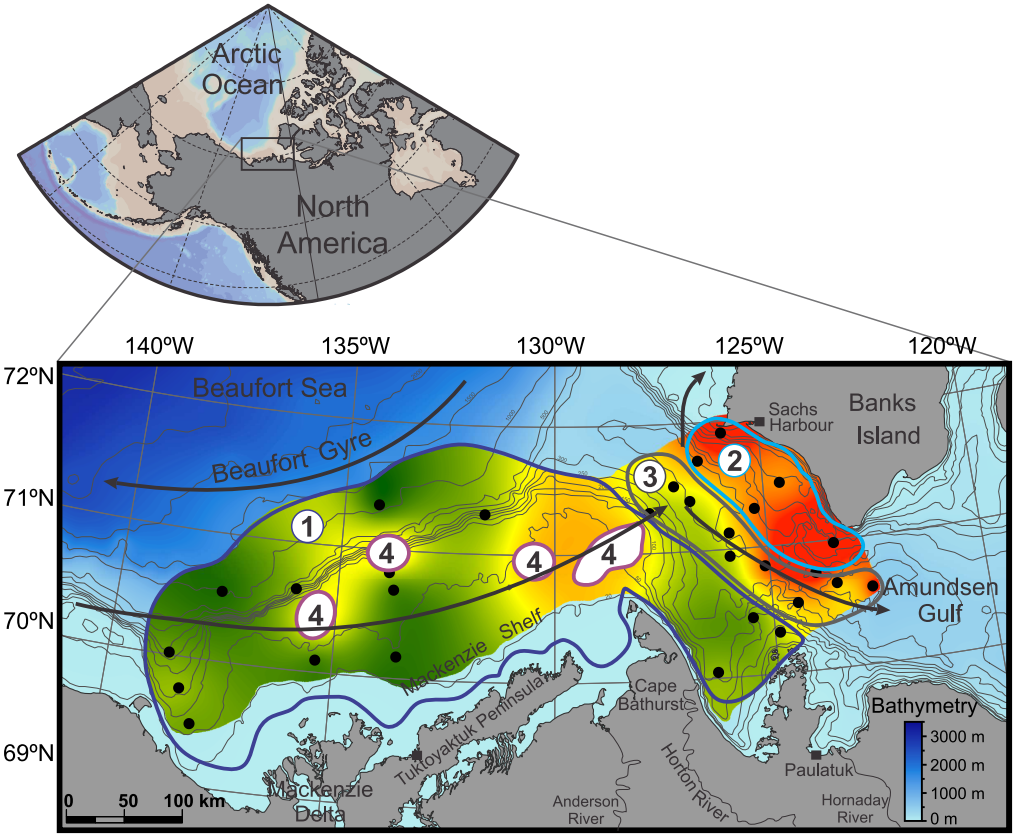

Sedimentary provinces:

1. Preferential influence of discharge of the Mackenzie River
   high phyllosilicates, Fe oxides, magnetite and Al-K-Ti-Fe-Cr-V-Zn-P contents
2. Preferential influence of coastal erosion
   high dolomite, K-feldspar and Ca-Mg-LOI contents
3. Transition zone (mixture characteristics from zones 1 and 2)
   intermediate phyllosilicates, magnetite, K-feldspar, dolomite, and Al-K-Ti-Fe-Mn-V-Zn-Sr-Ca-Mg-LOI contents
4. Zone influenced by mud volcanoes
   high quartz-plagioclase-authigenic carbonates and Si-Zr contents, high magnetic susceptibility